Performance of Mixture-Ratio-Controlled Hybrid Rockets under Uncertainties in Fuel Regression

Performance of Mixture-Ratio-Controlled Hybrid Rockets under Uncertainties in Fuel Regression

Kohei Ozawa[1] and Toru Shimada[2]
Institute of Space and Astronautical Science, JAXA, Sagamihara, Kanagawa, Japan, 252-5210

This paper evaluates various sources of oxidizer-to-fuel-mass-ratio (O/F) shifts in hybrid rockets and paths (physical phenomena) through which these O/F shifts affect flight performance. Moreover, the performance increase of O/F-control in hybrid rockets is evaluated. Vertical launches of O/F-uncontrolled and O/F-controlled of hybrid sounding rockets were simulated under two uncertainty models of fuel regression behavior based on experimental data: a) systematic errors with a constant deviation within $\pm 3\sigma$; b) random errors subject to a probability distribution. These simulations included all sources of O/F shifts that originated in the fuel regression behavior, and all paths through which the O/F shifts affect flight performance. Residual propellant mass and decreases in specific impulse are found to be the dominant causes of performance loss under both uncertainty models. For both cases a) and b), the O/F-controlled hybrid rockets maintained the performance expected under nominal fuel regression behavior, whereas the O/F-uncontrolled hybrid rockets had a lower performance by upwards of 6.69 % and 4.06 % in ΔV for cases a) and b), respectively. For case b), 3008 flight simulations revealed that the worst case of the O/F-controlled hybrid rocket had a 4.06 to 4.49% larger ΔV and 10.5 to 13.3% higher apogee than that of the O/F-uncontrolled hybrid rocket, and that the O/F-uncontrolled hybrid rocket had a 6.61 times larger standard deviation in ΔV. These results mean that the elimination O/F shift in hybrid

---

Kohei Ozawa and Toru Shimada, Flight Performance Simulations of Vertical Launched Sounding Rockets Using Altering-Intensity Swirling-Oxidizer-Flow-Type Hybrid Motors, July 23, 2015, Orlando, FL, AIAA 2015-3832.
Kohei Ozawa and Toru Shimada, Effects of O/F Shifts on Flight Performances of Vertically Launched Hybrid Sounding Rockets, July 7, 2017, Atlanta, GA, AIAA 2017-5051.

[1] Assistant Professor, Department of Mechanical and Control Engineering, Faculty of Engineering, Kyushu Institute of Technology, 1-1, Senshi-cho, Tobata-ku, Kitakyushu City, Fukuoka, Japan, 804-8550, AIAA Member.
[2] Professor, Department of Space Flight Systems, Institute of Space and Astronautics, Japan Aerospace Exploration Agency, 3-1-1, Yoshinodai, Chuo-ku, Sagamihara City, Kanagawa, AIAA Associate Fellow.

rockets significantly improves performance, as well as the accuracy and reliability of performance predictions.

Nomenclature

a = regression rate coefficient

A = cross-sectional area [m^2]

$\boldsymbol{A}$ = a matrix in the multiple regression theory

a_0 = regression rate coefficient for axial hybrid rockets

a_{ij} = the element of matrix $\boldsymbol{A}$ in i-th row and j-th column

AR = total aspect ratio including oxidizer tank and solid fuel [-]

$\boldsymbol{B}$ = estimated coefficient vector in multiple regression theory

$\boldsymbol{E}$ = resultant deviation vector

e_i = i-th element of $\boldsymbol{E}$

G = mass flux [kg/m^2s]

$\overline{I_{sp}}$ = time-averaged specific impulse [s]

L = length [m]

L^* = characteristic length [m]

L_o = length of oxidizer tank [kg]

m = mass [kg]

$\dot{m}$ = mass flow rate [kg/s]

n_1, n_2 = regression rate exponents corresponding to oxidizer mass flux and geometric swirl number [-]

O/F = oxidizer-to-fuel mass ratio [-]

r = radius [mm]

$\dot{r}$ = regression rate [m/s]

R_c = gas constant at chemical equilibrium inside the combustion chamber [J/kgK]

s = pseudorandom number subject to the normal distribution

S_g = geometric swirl number [-]

t = time [s]

T_c = temperature at chemical equilibrium inside the combustion chamber [K]

$t_{\alpha/2,i}$ = i-th Student's t-distribution of the two-sided probability of α

u = gaseous velocity [m/s]

x = residual propellant mass to initial propellant mass ratio

$\boldsymbol{x}$ = experimental condition vector $\left(1 \quad \ln \overline{G_o} \quad \ln\left(1+S_g^2\right)\right)^T$

$\boldsymbol{X}$ = ν-times experimental condition matrix

$\boldsymbol{Y}$ = column vector of ν-times experimental results

$\boldsymbol{\beta}$ = coefficient vector of regression rate coefficient and exponents $(\ln \overline{a_0} \quad n_1 \quad n_2)^T$

γ = specific heat ratio at chemical equilibrium inside the combustion chamber [-]

ΔV = total acceleration of propulsive subsystem, $\int_{t_i}^{t_f}(F/m)dt$ where F and m are thrust and mass of the rocket, respectively.

η_{c^*} = c^* efficiency [-]

μ = dimension of $\boldsymbol{\beta}$ [-]

ν = number of fuel regression rate data [-]

ρ = density [kg/m^3]

σ = standard deviation

τ = staying timescale inside the combustion chamber [s]

φ = radius ratio based on throat radius [-]

Subscripts

f = final

i = initial

in = inner side of a single port solid fuel grain

inj = injector

m = moment arm

o = oxidizer

out = outer side of a single port solid fuel grain

p = fuel port

pc = pre-combustion chamber

PMMA = polymethyl methacrylate

ref = referential

sf = solid fuel

t = nozzle throat

WAX = paraffin wax

$\bar{}$ = nondimensional

I. Introduction

Shifts of oxidizer-to-fuel-mass ratio (O/F) occur in conventional hybrid rocket propulsion. This phenomenon is called “O/F shift”. There are a few types of mechanisms that cause O/F shifts in hybrid rockets, but no discussions of them were found in previous studies. Most previous studies simply conclude with the notion that port expansion and throttling are the only causes of O/F shifts, and decreases the performance resulting from O/F shifts are only due to corresponding shifts in the thermodynamic state of the product gas, which affect ideal c^* and exit velocity [1][2][3][4]. Altman et al.[3] and Karabeyoglu et al.[4] concluded that O/F shifts are negligible, or that the resulting shifts in enthalpy only cause considerable performance loss under deep throttling.

However, there are a few studies which challenge such conventional theories. Barato et al. [5] evaluated the performance loss due to residual propellant mass which results from a constant deviation in the modeled fuel regression curve from the actual one. In other words, their study proposes that the error of the fuel regression model is another source of O/F shifts, and residual propellant mass is another factor of performance loss, but the scale of the error was not based on experiment results. Casalino et al. [6][7][8] have investigated the optimal and robust design given some uncertainty in fuel regression behavior in hybrid rocket propulsion, for the development of an alternative upper stage of the Vega launcher, or a nano-satellite airborne launch vehicle. Their sensitivity analysis revealed that the uncertainty of fuel regression behavior has one of the strongest and non-linear effects on performance in the design of the hybrid rocket upper stage. Additionally, they found out that the expected and worst performances are improved when the propellant O/F is designed to be more fuel-rich than in the nominal operation so that residual oxidizer mass is minimized in the highest regression rate case. Ozawa and Shimada [9] also challenged the conventional assumption that O/F shifts affect the propulsive performance only through the thermodynamic state of the product gas. Their flight

simulations under a nominal (median) fuel regression behavior clarified that O/F shifts caused the shifts in c* efficiency and nozzle throat erosion rate due to their dependency on O/F, and that c* efficiency has approximately a 30 % contribution to the total performance drop caused by the O/F shifts in hybrid sounding rocket missions.

The above studies which contended with conventional assumptions illuminated other factors related to O/F shifts, but not all factors were integrated into the subsequent evaluations. This study has two purposes: 1) classifying the sources of O/F shifts and their paths towards affecting flight performance; 2) evaluating the effects of O/F shifts on the comprehensive performance of hybrid rocket propulsion, including O/F shifts due to the fuel regression uncertainty and the physical phenomena affected by O/F shifts.

This investigation begins by classifying various sources of O/F shifts and the paths through which the O/F shifts affect flight performance. After this classification, fuel regression behaviors are modeled with uncertainty based on experimental results. This paper implements two uncertainty models, for: a) systematic errors with a fixed scale of deviation; b) random errors with a probability distribution. The systematic and random errors were assumed to correspond to the dispersion in the manufacturing and operating environment of the engine, and the randomness included in the turbulent combustion and entrainment mass transfer of the liquefying fuel, respectively. These fuel regression models are used to evaluate the performance increase of O/F-controlled hybrid sounding rockets over their O/F-uncontrolled counterparts. In this study, the Altering-intensity Swirling Oxidizer Flow Type (A-SOFT) [11] method was implemented as the O/F control method because of its combustion stability and high baseline of regression rates. As shown in Fig. 1, A-SOFTs have axial and tangential injectors, of which oxidizer mass flow rates are independently controlled. This “dual injector” makes it possible to control both thrust and O/F by using the dependency of regression rates on geometric swirl number and oxidizer port mass flux. Swirling Oxidizer Flow Type (SOFT) [12] hybrid sounding rockets were implemented as the O/F-uncontrolled counterpart of the A-SOFT configuration. SOFT hybrid rockets have similar regression rates, but only tangential oxidizer injection such that thrust and O/F cannot be controlled simultaneously.

To evaluate the significance of O/F control, this study expands the flight simulations of the vertical ascent of single-stage sounding rockets under nominal fuel regression [9] by implementing the two types of fuel regression errors previously mentioned. In these simulations, the thrust is controlled to achieve an altitude as high as possible with a finite mass of propellant and throttle range, considering the effects of gravitational acceleration and aerodynamic drag dependent on the state vector of the rocket. For the random error cases, more than 3000 flights are

simulated to statistically analyze the expected (median) and guaranteed (the worst) performance of both types as well as the deviations of the results. The simulated flight performances of O/F-controlled and –uncontrolled hybrid rockets are compared, and the performance losses related to O/F shift are analyzed to build an understanding of the proportions of the respective factors to the total performance loss of the hybrid rockets.

II. Classification of O/F Shifts and Effects on Hybrid Rocket Propulsion

Before investigating and evaluating the effects of O/F shifts, it is necessary to classify their sources as well as the physical phenomena related to O/F shifts in the context of hybrid rocket engines for meaningful evaluations of the effects of O/F shifts on flight performance. These classifications are summarized in Fig. 2. The items listed in this figure are discussed in detail in the following subsections.

A. Various Sources of O/F Shifts

O/F shifts are caused by both the oxidizer feed system and solid fuel regression behavior. The former type of O/F shift is not deeply discussed in this paper because errors in liquid propellant supply also occur in liquid rocket propulsion, and currently, they are not recognized as a serious problem because additional propellants for off-nominal performance are included in the propellant budget of a typical liquid rocket [10]. On the other hand, the latter source of O/F shift is unique to hybrid rocket propulsion, and has not been deeply discussed over the long research history of hybrid rockets. Moreover, conventional hybrids cannot avoid this type of O/F shift because fuel mass flow rates of conventional hybrids are not controlled independently of oxidizer flow rates or thrust.

O/F shifts due to solid fuel regression behavior can be classified into those associated with a nominal (median) regression rate equation and those caused by errors from the nominal behavior. The former O/F shifts are caused by the following nonlinear dependence of fuel regression rates on oxidizer mass flux:

$$\dot{r} = aG_o^{n_1} \tag{1}$$

where $\dot{r}$, a, G_o, and n_1 refer to fuel regression rate, a constant coefficient, oxidizer mass flux, and a constant exponent, respectively. n_1 typically ranges from 0.5 to 0.8 for most of the combinations of propellants. For a single circular port, Eq. (1) provides the following expression of O/F:

$$O/F = \frac{\dot{m}_o{}^{1-n_1} r_p^{2n_1-1}}{2\pi^{1-n_1} a L_{sf} \rho_{sf}} \tag{2}$$

where $\dot{m}_o$, r_p, L, and ρ_f refer to oxidizer mass flow rate, port radius, port length, and solid fuel density, respectively. This equation suggests that throttling and fuel port expansion cause O/F shifts dependent on the constant n_1. These types of O/F shifts have been discussed in previous studies [1][2][3], however, the discussions in these studies implicitly assume that a motor operates only for a single purpose, and only along a single thrust curve. Under this assumption, all papers concluded that O/F shifts due to deep throttling can cause a considerable loss of propulsive performance, but those due to port diameter expansion do not cause significant problems.

O/F shifts are also caused by deviations in fuel regression from the nominal (median) fuel regression rate equations, an important topic which few studies have considered. This investigation assumes that these types of O/F shifts can be further classified into two categories based on the types of errors in the fuel regression. The first type is caused by systematic errors in the nominal regression rate equation themselves, which refer to a shift in the median regression behavior during a flight from that estimated by firing tests. Both studies by Barato et al. [5] and Casalino et al. [6] assumed a few percent errors in a and n of Eq. (1). The other candidate is a random error, which has been completely overlooked in performance evaluations of hybrid rockets until now. This type of error refers to the random variance of instantaneous regression rates from the median equation, and should be modeled as a random variable subject to a probability distribution. In the presence of random errors, the performance of the rocket should also have a probability distribution. The performance loss due to these two fuel regression errors are characterized especially by the yield of residuals, and these regression errors are hardly considered in median flight performance predictions except for the previous works referred above. There can be secondary O/F shifts due to the oxidizer mass flow rate shifts coupled with pressure shifts at the combustion chamber shifts as a result of the O/F shifts caused by the fuel regression behavior. However, this study did not consider these coupling problems related to the oxidizer feed system. The paths decreasing the flight performance are discussed in the next subsection in more detail.

B. Effects of O/F Shifts on Performance

The paths through which O/F shifts affect flight performance are shown on the right side of Fig. 2. These paths can be classified into those related to propulsive performance and those directly affecting flight performance.

A dominant path affecting the propulsive performance is the shift in the thermodynamic state and molecular fractions of the product gas per unit mass. This shift affects the characteristics of the ideal engine performance. In several previous papers [1][2][3], this impact was expected to be small or negligible under constant thrust, but c^* is expected to decrease by up to 10% from the reference c^* under deep throttle rates [3]. The nominal performance

evaluation of O/F-controlled and –uncontrolled hybrid rockets by Ozawa and Shimada [9] revealed that this type of loss has the largest impact when assuming median regression behavior.

The second important path is a shift in c^* efficiency. One of the major parameters correlated with c^* efficiency is L^*, as an indicator showing the completeness of the combustion reaction in the chamber. This is because L^* characterizes the residence time of the propellants inside the combustion chamber. The ideal L^* to complete the combustion should depend on O/F because the ideal L^* should be evaluated by the velocity of the product gas dependent on O/F. Ozawa and Shimada [9] also revealed that the shifts in c^* efficiency are the second most important path through which O/F shifts decrease the propulsive performance when assuming median regression behavior.

The third path is the throat erosion of carbon-based nozzles such as graphite, which are typically adopted in hybrid rocket propulsion. O/F shifts change the mole fractions of oxidizing species for graphite in the core flow at the throat, predominantly; O_2, O, OH, H_2O, and CO_2 [11], leading to shifts in throat erosion rates. Moreover, we can easily understand that the shifts in erosion rates should secondly affect L^* of the combustion chamber due to the shifts in the time history of the nozzle throat area. Ozawa and Shimada [9] revealed that the shift in throat erosion is the least important path in these three paths for the median regression behavior.

In addition to these three paths, the flight performance is also affected by propellant residual resulting from the accumulation of fuel regression errors during engine operations, when considering the uncertainties of regression rate models. This is the fourth path through which O/F shifts affect flight performance. This path tends to be overlooked in the evaluation of O/F shifts because this phenomenon does not affect propulsive performance like specific impulse, but it does directly affect flight performance through increases in final mass and decreases in the effective propellant mass. Barato et al. [5] reported that, under the presence of a few percents of systematic error in the constants of the regression rate equation, the residuals cause a large impact on flight performance, though the scale of systematic errors was not validated by any experimental data.

O/F shifts and propellant residual can also occur as a result of the accumulation of random errors in the fuel regression behavior, which seem to be more important because the random errors should remain to some degree even after a strict quality control of the propulsion system. However, no investigation was found on this topic.

III. Modeling of Fuel Regression Behavior with Uncertainty

In this section, fuel regression rate behavior is analyzed from previous experimental data, and the fuel regression behavior for SOFTs and A-SOFTs is modeled. In our flight simulations, paraffin wax and gaseous oxygen (GOX; stored as liquid phase) are selected as the propellants because of high baselines of regression rates. However, there is little previous data with paraffin wax and GOX available to model the dependence on swirl number. The two papers by Shinohara et al. [14] and Saito et al. [15] reported that paraffin-based fuels have a higher sensitivity to geometric swirl number than other conventional fuels, especially in the front region of the grain. Despite these valuable results, it remains too difficult to model a reliable fuel regression behavior only with this data due to small numbers of experimental conditions and data. Therefore, in this section, we analyze the medians and uncertainties of the axially-injected hybrid rockets with a wax-based fuel and the swirling hybrid rockets with polymethyl methacrylate (PMMA) using multiple regression analysis, and we model a "virtual" fuel regression behavior of the wax-based fuel with a sensitivity to swirl strength by combining the results of these two analyses in the same way as our previous modeling [9]. The experimental data used includes various experimental conditions in terms of the dimensions of motors and the time history of the oxidizer mass flux. Therefore, the uncertainty models in this paper are probably larger than the actual uncertainty of a specific type of engine. This is because, typically, there would be many firing tests under a specific test condition with the acceptable errors in the specifications of the engine and the time history of oxidizer mass flow rate over the development, as a part of qualification test. However, previous literature does not clarify the relationship between the strength of the quality control and the uncertainty in fuel regression. At least, the regression uncertainty modeled in this paper can be regarded as the initial worst behavior of dispersion considered before quality control.

We used the following regression rate equation for both SOFTs and A-SOFTs [13]:

$$\dot{r}(t) = a_0 G_o(t)^{n_1} \left\{1 + S_g(t)^2\right\}^{n_2} \tag{3}$$

where S_g refers to geometric swirl number to characterize the swirl strength of the injected oxidizer. a_0 and n_2 refer to the regression rate coefficient for $S_g = 0$ and a constant exponent characterizing the sensitivity to S_g. It should be noted that Eq. (3) is also an extension of the fuel regression rate equation for axially injected hybrid rockets [16]. Geometric swirl number is defined as the following equation as

$$S_g = \frac{r_m \rho_{inj} u_{inj}^2 A_{inj}}{r_{pc} \rho_{inj} u_{pc}^2 A_{pc}} = \frac{r_m A_{pc}}{r_{pc} A_{inj}} \tag{4}$$

where r_m refers to the moment arm of the injector ports, the subscripts "*inj*" and "*pc*" refer to injector port and pre-chamber, respectively. u_{pc} refers to the axial velocity of oxidizer in the pre-combustion chamber. The transformation to the right hand in above equation assumed incompressible oxidizer flows and the mass conservation law of $\rho_{inj} u_{inj} A_{inj} = \rho_{inj} u_{pc} A_{pc}$. It was experimentally shown that this type of equation also successfully approximates the fuel regression behavior of A-SOFTs when polypropylene (PP) and GOX are used as propels [11].

A. **Multiple Linear Regression Analyses of Fuel Regression Behaviors**

The datasets of regression rates are the time- and space-averaged values, but the fuel regression models constructed are used as instantaneous space-averaged regression behaviors in the flight simulations. In our analysis, the uncertainty of the individual sample data points was ignored for simplicity. It is also assumed that the mean and the standard deviation of the population of the fuel regression data are unknown. The experimental conditions differ for each regression rate measurement in terms of the dimensions of the engines and solid fuel grains, the injector designs, and the time histories of oxidizer mass flow rates so that it is appropriate to regard the characteristics of the dispersion in the regression behavior as that before the quality control of a specific engine.

The multiple linear regression method [17] was used to evaluate the uncertainties of the two types of fuel regression behaviors. This method is characterized by dividing the deviations of the median equation into the uncertainties in the median values of a_0, n_1, and n_2 (the range of confidence interval, CI [17]) and remaining random dispersions with Gaussian probability distributions (the two side gaps between the prediction interval, PI [17], and confidence interval), assuming that the model equation acquired cannot perfectly explain the characteristics of the fuel regression behavior. Considering these characteristics of the two intervals, as well as the above assumptions, it is appropriate that the systematic and random error models are constructed by using CIs and PIs, respectively.

The multiple linear regression using Eq. (3) assumes that the *i*-th experimental result can be expressed with the following equation as

$$\ln \overline{\dot{r}_i} = (\ln \overline{a_0} \quad n_1 \quad n_2) \left(1 \quad \ln \overline{G_{o_i}} \quad \ln\left(1 + {S_{g_i}}^2\right)\right)^T + e_i \tag{5}$$

where $\overline{\dot{r}_i}$, $\overline{G_{o_i}}$, $\overline{a_0}$, and e_i are $\dot{r}_i/\dot{r}_{ref}$, $G_{o_i}/G_{o_{ref}}$, $a_0/a_{0_{ref}}$, and the remaining deviation that cannot be modeled with Eq. (3), respectively. The subscript "ref" means a reference variable to nondimensionalize the fuel regression equation. The reference numbers have $\dot{r}_{ref} = a_{0_{ref}} G_{o_{ref}}^{n_1}$,where the term $a_{0_{ref}}$ is determined by the least-squares method. In this paper, $G_{o_{ref}}$ was selected as the mean oxidizer mass flux of the experimental dataset. It is noted that the constants

$(\ln \overline{a_0} \quad n_1 \quad n_2)$ are common to all experiments. For axial hybrid rockets, the first term of the right hand becomes a two-dimensional vector without n_2 or $\ln\left(1 + {S_{g_i}}^2\right)$. Now, let us suppose n experiments subject to Eq. (5). The results of ν-times experiments can be summarized by

$$\boldsymbol{Y} = \boldsymbol{X\beta} + \boldsymbol{E} \tag{6}$$

where $\boldsymbol{Y}$, $\boldsymbol{\beta}$, and $\boldsymbol{E}$ refer to the column vectors of the resultant regression rates $(\ln \bar{r}_1 \quad \ln \bar{r}_2 \quad \ldots \quad \ln \bar{r}_\nu)^T$, the constant coefficient vector $(\ln \overline{a_0} \quad n_1 \quad n_2)^T$, and the resultant deviation $(e_1 \quad e_2 \quad \cdots \quad e_\nu)^T$ subject to a normal distribution, respectively. $\boldsymbol{X}$ refers to the $\nu \times 3$ matrix of the experimental conditions. According to the multiple regression analysis theory [17], the estimated coefficient vector $\boldsymbol{B} = E(\boldsymbol{\beta})$ is expressed as

$$\boldsymbol{B} = (\boldsymbol{X}^T\boldsymbol{X})^{-1}\boldsymbol{X}^T\boldsymbol{Y} \tag{7}.$$

The sum of squared residuals (SS_R) and the variance of Y (σ) have the following relation as

$$SS_R = (\nu - \mu)\sigma^2 = \sum_{i=1}^{\nu}(\boldsymbol{Y}_i - \boldsymbol{X}_i\boldsymbol{B})^2 = \boldsymbol{Y}^T\boldsymbol{Y} - \boldsymbol{B}^T\boldsymbol{X}^T\boldsymbol{Y} \tag{8}$$

where μ is the dimension of the model equation, therefore, μ = 2, 3 for axial and swirling hybrids, respectively. The CI is defined as the range where the median linear relation of Eq. (5) is estimated to be located with the two-sided probability of α. The borders of the CI are

$$\ln \bar{r} = \boldsymbol{Bx} \pm \sqrt{\frac{SS_R\boldsymbol{x}^T(\boldsymbol{X}^T\boldsymbol{X})^{-1}\boldsymbol{x}}{\nu-\mu}}\, t_{\frac{\alpha}{2},\nu-\mu-1} = \boldsymbol{Bx} \pm \sigma\sqrt{\boldsymbol{x}^T(\boldsymbol{X}^T\boldsymbol{X})^{-1}\boldsymbol{x}}\, t_{\frac{\alpha}{2},\nu-\mu} \tag{9}$$

where x refers to the vector of the experimental conditions, and $t_{\frac{\alpha}{2},\nu-\mu}$ refers to the $\nu - \mu$th Student's t-distribution [18] with the two-sided probability of α, considering the sample size is small. In this study, the CI is used for the estimated median fuel regression behavior with a fixed error from the true median fuel regression behavior because the CI represents the existence probability of the population means.

The PI refers to an estimated existing area of the median linear relation between x and y with a two-sided probability of α. The upper and lower limits of the PI are

$$\ln \bar{r} = \boldsymbol{Bx} \pm \sigma\sqrt{1 + \boldsymbol{x}^T(\boldsymbol{X}^T\boldsymbol{X})^{-1}\boldsymbol{x}}\, t_{\frac{\alpha}{2},\nu-\mu} \tag{10}.$$

The range of the PI is larger than the CI by $2\sigma\left\{\sqrt{1 + \boldsymbol{x}^T(\boldsymbol{X}^T\boldsymbol{X})^{-1}\boldsymbol{x}} - \sqrt{\boldsymbol{x}^T(\boldsymbol{X}^T\boldsymbol{X})^{-1}\boldsymbol{x}}\right\} t_{\frac{\alpha}{2},\nu-\mu}$ because the PI includes the variance of e in Eq. (5). Therefore, Eq. (10) is modified to be used for the fuel regression behavior with a random error subject to a probability distribution in this study.

The total 69 fuel regression data of axial hybrids with paraffin wax and GOX were analyzed according to this theory. The result of the CI was

$$\ln \bar{\dot{r}}_{WAX} = -1.39 \times 10^{-15} + 0.640 \ln \overline{G_o}_{WAX} \pm \sigma_{WAX} \sqrt{\boldsymbol{x}^T (\boldsymbol{X}^T \boldsymbol{X})^{-1} \boldsymbol{x}} t_{\frac{\alpha}{2},67}$$
$$\sigma^2_{WAX} = 4.61 \times 10^{-3}, (\boldsymbol{X}^T \boldsymbol{X})^{-1} = \begin{pmatrix} 17.7 & 7.29 \\ 7.29 & 16.7 \end{pmatrix} \times 10^{-3} \tag{11}$$

where $\dot{r}$ in [mm/s] is approximated with G_o in [kg/m^{2}s]. Note that the border corresponding to 3σ shifts by 4% even for the 67th t-distribution: 3.12. In Fig. 3, the borders of the PIs and CIs with the two-sided probabilities corresponding to those of 3σ in normal distribution are compared with the experimental results.

The fuel regression datasets by Yuasa's group [12] were used for the linear regression analysis of SOFTs with PMMA and GOX. These papers show a total of 45 data points in a relatively small range of oxidizer mass flux with 5 options for geometric swirl numbers. The result of the CI was

$$\ln \bar{\dot{r}}_{PMMA} = 9.12 \times 10^{-16} + 0.616 \ln \overline{G_o}_{PMMA} + 0.156 \ln\left(1 + S_g^2\right) \pm \sigma_{PMMA} \sqrt{\boldsymbol{x}^T (\boldsymbol{X}^T \boldsymbol{X})^{-1} \boldsymbol{x}} t_{\frac{\alpha}{2},42}$$
$$\sigma^2_{PMMA} = 4.13 \times 10^{-4}, (\boldsymbol{X}^T \boldsymbol{X})^{-1} = \begin{pmatrix} 319 & 26.3 & -57.3 \\ 26.3 & 303 & 5.98 \\ -57.3 & 5.98 & 15.0 \end{pmatrix} \times 10^{-7}, t_{\frac{\alpha}{2},42} = 3.19 \tag{12}$$

where $\dot{r}$ in [mm/s] was approximated with G_o in [kg/m^{2}s]. The border corresponding to 3σ shifts by more than 6% for the 42nd t-distribution: 3.19. In Fig. 4, the borders of the PIs and CIs with the two-sided probabilities corresponding to those of 3σ in normal distribution are compared with the experimental results.

As mentioned above, their uncertainty models of SOFTs were modeled from the two fuel regression behaviors analyzed in the above paragraphs because there was not enough data for swirling hybrid rockets using paraffin and GOX as propellants. In this paper, the regression rate coefficient, exponent, and all components in the covariance matrix of paraffin and GOX in Eq. (11) were used without any modifications for the artificial regression behavior because the first 2×2 component in the matrix of $\sigma^2_{WAX}(\boldsymbol{X}^T \boldsymbol{X})^{-1}$ does not include any information about the swirling flows of Eq. (3). On the other hand, the geometric swirl number exponent m and the remaining components correlated with geometric swirl number were quoted from those in Eq. (12), because these remaining parameters should be related to the sensitivity of fuel regression behavior to geometric swirl number. Hence, the confidence interval of SOFTs assuming paraffin and GOX is modeled as

$$\bar{\dot{r}}_{WAX} = \exp(-1.39\times10^{-15})\,\overline{G_{o_{WAX}}}^{0.640}\left(1+S_g^2\right)^{0.156} \times \exp\left(\pm\sqrt{\boldsymbol{x}^T\boldsymbol{A}\boldsymbol{x} + 2a_{23}\ln\left(\frac{G_{oref_{WAX}}}{G_{oref_{PMMA}}}\right)\boldsymbol{x}_3}\,t_{\frac{\alpha}{2},67}\right)$$

$$\boldsymbol{x} = \begin{pmatrix} 1 \\ \ln\overline{G_{o_{WAX}}} \\ \ln\left(1+S_g^2\right)\end{pmatrix}, \boldsymbol{A} = \begin{pmatrix} a_{11} & a_{12} & a_{13} \\ a_{21} & a_{22} & a_{23} \\ a_{31} & a_{32} & a_{33}\end{pmatrix} \quad (13).$$

$$\begin{pmatrix} a_{11} & a_{12} \\ a_{21} & a_{22}\end{pmatrix} = \sigma_{WAX}^2(\boldsymbol{X}_{WAX}^T\boldsymbol{X}_{WAX})^{-1}$$

$$a_{31} = a_{13} = \sigma_{PMMA}^2[(\boldsymbol{X}_{PMMA}^T\boldsymbol{X}_{PMMA})^{-1}]_{(1,3)}$$

$$a_{32} = a_{23} = \sigma_{PMMA}^2[(\boldsymbol{X}_{PMMA}^T\boldsymbol{X}_{PMMA})^{-1}]_{(2,3)}$$

$$a_{33} = \sigma_{PMMA}^2[(\boldsymbol{X}_{PMMA}^T\boldsymbol{X}_{PMMA})^{-1}]_{(3,3)}$$

where the 67th t-distribution was used for the two-sided probability model as in Eq. (11). The second term in the square root is needed to adjust the sensitivity of a_{23}, which was derived using the referential oxidizer mass flux of PMMA. This confidence interval was used as the systematic error model in the flight simulations because the definition of systematic error is similar to that of confidence interval in terms of the uncertainty of median regressed equations.

The fuel regression model with random errors was created by modifying the prediction interval model. In this paper, the random dispersions in the CIs are assumed to simulate those in the entrainment of the melted wax and the various transport phenomena related to the turbulent combustion. The prediction interval model was created by replacing σ^2 and $\sigma^2(\boldsymbol{X}^T\boldsymbol{X})^{-1}$ by σ_{WAX}^2 and $\boldsymbol{A}$ in $\sigma\sqrt{1+\boldsymbol{x}^T(\boldsymbol{X}^T\boldsymbol{X})^{-1}\boldsymbol{x}}$ of Eq. (10), respectively. In addition to this modeling, the fuel regression model with random errors was made by adding the pseudorandom number subject to the normal distribution as follows:

$$\bar{\dot{r}}_{WAX} = \exp(-1.39\times10^{-15})\,\overline{G_{o_{WAX}}}^{0.640}\left(1+S_g^2\right)^{0.156}\exp\left(s\sqrt{\sigma_{WAX}^2 + \boldsymbol{x}^T\boldsymbol{A}\boldsymbol{x} + 2a_{23}\ln\left(\frac{G_{oref_{WAX}}}{G_{oref_{PMMA}}}\right)\boldsymbol{x}_3}\right) \quad (14)$$

where s refers to the pseudorandom error subject to the normal distribution when $\sigma = 1$.

Figure 5 shows the virtual fuel regression rate model with the $\pm3\sigma$ boundaries of the systematic and random errors. These models are equivalent to the CI and PI, respectively, except for the replacement of the t-distribution by normal distribution for the random error model so that these models draw the same curves when $\boldsymbol{x_3} = S_g = 0$. The sizes of the 3σ error were at most 6.21% and 24.6% in the range of oxidizer mass flux from 10 to 500 [kg/m^{2}s] and geometric swirl number from 0 to 20, respectively. The size of the systematic error has a dependence on operating condition because $\boldsymbol{x^T A x}$ is the only factor to characterize the systematic error. In the range of G_o from 40 to 120 [kg/m^{2}s], the

3σ error was less than 3% because there were many sample data in this range of operating conditions. On the other hand, the random error model is less sensitive to operating conditions because σ_{WAX} has the dominant scale in the random error term in Eq. (14). It should be also noted that the -3σ error varies between 19.2 and 19.7% whereas the $+3\sigma$ error ranges between 23.7 and 24.6%. This asymmetry in error values occurs because the linear regression analysis was carried out after taking the logarithm of the experimental data.

IV. Hybrid Sounding Rocket Flight Simulation

The flight performances of O/F-controlled and –uncontrolled hybrid sounding rockets are compared, using an in-house flight simulation code capable of evaluating the effects of O/Fs on the chemical equilibrium, c* efficiency, and nozzle throat erosion rates, and considering fuel regression rate uncertainties. This flight simulation was developed by modifying the subroutine of fuel regression rate calculation of the in-house code to evaluate the performance of hybrid sounding rockets with an O/F control under the median fuel regression behavior [9]. In this study, the fuel regression behavior has an uncertainty expressed as Eq. (13) or (14). Except for the fuel regression models, all subroutines remained unchanged. The initial conditions and environment parameters like mass fractions, dimensions, throttling range of the rockets, atmosphere, and gravity also remained unchanged. These parameters are explained in detail in Ref. [9]. This section presents a modified block diagram and the simulated cases, in addition to a brief explanation of the previous flight simulation code.

A. Hybrid Rocket Engine Model

The flight simulation code assumes that the hybrid rocket engine model is sensitive to O/F through the dependency of the theoretical thermodynamic state of the product gas, nozzle throat erosion, and c* efficiency on O/F.

The theoretical thermodynamic state is determined at the O/F calculated by the oxidizer mass flow rate, fuel regression rate behavior, and temporary chamber pressure, using an in-house subroutine assuming the chemical equilibrium of 11 chemical species. This subroutine was developed by referring to the technical report of Gordon and McBride [19]. The resultant propellant mass flux calculated by the thermodynamic state and the choking condition at the nozzle throat is iterated until the input value matches the output value within a threshold of 0.1%.

Throat erosion rate is calculated with a model assuming a balance between the oxidizing species supply from the core flow and the chemical throat erosion of the graphite nozzle through the concentration boundary layer. In this model, the oxidizing species and products were assumed to be transported by Fick's law, and the concentration

boundary layer is scaled by the Gilliland-Sherwood equation [20]. The boundary condition at the core flow is given by the thermodynamic state and the mole fraction under the equilibrium sonic condition, and that at the throat surface is given by the reaction rate model of the graphite with the oxidizing species. This model has a good agreement with experimental throat erosion rates at instantaneously changing conditions [21], as shown in Fig. 6. The experimental data being referenced did not include throat temperature so the results of the erosion rate model are shown for a range of throat temperatures. The experimental results appear to be more sensitive to equivalence ratio than the model results. However, this is most likely the effect of the transient throat temperature. In this reference data, throat temperature is not necessarily the same for two points with the same equivalence ratio and thus the effect of throat temperature is not being represented. In this flight simulation, we used the throat erosion model with the throat surface temperature of 3000 [K] to maximize the effect of throat erosion on performance and the dependency of throat erosion on O/F.

Regarding the c^* efficiency model, our approach is to relate a gaseous velocity scale with c* efficiency as well as L^*. For liquid rocket propulsion, the approach usually adopted for handling L^* was taken due to the lack of other approaches. For liquid propulsion, c^* efficiency is typically related to the characteristic chamber length L^* [22] as a factor for characterizing the residence time inside the combustion chamber to relate mixing (and diffusion) and chemical reaction rates with the design of the combustion chamber. However, the typical approach to characterize c* efficiency only with L* implicitly requires the assumption that the velocity scale inside the chamber is independent of operating conditions. It is reasonable to assume that the gaseous velocity scale depends on O/F, especially for hybrid rocket propulsion. So c* efficiency was evaluated as a function of the timescale of L* and the velocity scale in our flight simulations. Here the ideal velocity of the product gas, which depends on O/F, is used as the gaseous velocity scale. This combination can give a residence timescale, which is the original concept of the characterization of c* efficiency, by dividing L* with the velocity scale. The resultant residence timescale τ in our model can be shown as

$$\tau = \frac{L^*}{\sqrt{\gamma R_c T_c}} \left(\frac{\gamma+1}{2}\right)^{\frac{\gamma+1}{2(\gamma-1)}} \tag{15}$$

where L^* is a characteristic length of the combustion chamber, and γ, R_c, and T_c are specific heat ratio, gas constant, and temperature of the product gas at chemical equilibrium in the combustion chamber. Note that the governing phenomena of hybrid rocket combustion include mixing and chemical reactions. As of now, the first-order reaction rate function of the residence time is substituted as the form of the sensitivity of c* efficiency due to the lack of the mixing rate functions for boundary layer combustion. Also, in our c* efficiency model an empirical coefficient was added as an upper limit to the c* efficiency achieved without a mixing enhancer or an aft-chamber, to fit the results

of the large-scale firing experiments [16]. This coefficient was designed to have a linear dependency on geometric swirl number because swirling oxidizer injection increases c* efficiency [11][23]. As a result of curve fitting the experimental results of the axial and swirling hybrid rocket engines using paraffin-oxygen [16][23][24], the c* efficiency η_{c^*} was modeled as follows [9]:

$$\eta_{c^*} = \min\left[\left(8.03S_g + 825\right) \times 10^{-3}\{1 - \exp(-10.15 \times 10^2 \tau)\}, 1\right] \tag{16}$$

The min function to limit η_{c^*} equal to or less than 1 does not work until $S_g = 21.8$. In practice, such a large geometric swirl number is not expected to be used, because, for example, the maximum of the best performance cases for the nominal fuel regression behavior was S_g = 8.9. Figure 7 shows good agreement of the modeled c* efficiency with the experimental data. Most of the experimental results agree with the model equation to within $\pm$20%.

B. **Block Diagram**

Figure 8 shows the block diagram of the flight simulation. The simulation code starts with the calculations of the dimensions of the rocket from the given design parameters. The upper limit of oxidizer mass flow rate is also determined at this time based on the initial port diameter and the maximum oxidizer mass flux given as one of the initial conditions.

At the start of each time step, the code checks whether oxidizer and fuel remain in the rocket. If so, the code calculates the target thrust according to the thrust control law appropriate to the state vector of the rocket (velocity, altitude, and remaining mass) and the ambient pressure at that time. The thrust control law is based on the Pontryagin's maximum principle [25] to maximize the apogee of the rocket. If both remaining fuel and oxidizer mass are less than the target consumption, then it is completely spent at that time step. In the O/F-controlled rockets, the program sets the operating conditions of oxidizer mass flow rate and geometric swirl number by calculating the engine performance under the median fuel regression behavior, assuming the onboard computer (OBC) cannot predict uncertainties in the fuel regression rates, based on the target propellant mass flow rate. For the O/F-controlled types, the geometric swirl number for the next time step is assumed to be accurately determined using Eq. (3) so that the O/F in the chamber is equal to that of the remaining propellants at that time at a refresh rate of 10 [ms], including the delay of the valve control. For the O/F-uncontrolled types, the geometric swirl number is included in the fixed initial conditions, and the oxidizer mass flow rate is only calculated and controlled for the target thrust. The regression rate, throat erosion rate, and engine performance are calculated based on the operating conditions, and the fuel regression behavior with the

uncertainty model. The aerodynamic drag and gravity exerted on the rocket are calculated from the state vector of the rocket at that time. In the final part of the time step, the state vector is updated by the time-integration of the equation of motion with the fourth-order Runge-Kutta method. The remaining mass of the oxidizer, the fuel port diameter, and the throat diameter are time-integrated with the Euler method for simplicity and computing time. The time interval of these integrations is 10 [ms]. At the end of each time step, the switching parameter of the thrust control law is updated using the instantaneous specific impulse for the following time step. The powered flight continues until either the fuel or oxidizer is spent. After the engine cut-off, the flight simulation runs in free flight mode until the velocity of the rocket becomes negative.

The thrust control was limited by the nozzle flow separation limit and the thrust corresponding to the initial oxidizer mass flow rate. The closed-loop thrust (and O/F) control was simulated under the assumption that the OBC is capable of sensing fuel port and nozzle throat diameters, and estimating c* efficiency using the expected fuel and oxidizer mass flow rate, effective geometric swirl number, and the actual chamber pressure as well as the accurate state vector (position, velocity, and the remaining mass) of the rocket. In practice, real-time nozzle throat erosion measurements are possible using ultrasound sensors [26]. Similarly, an onboard real-time fuel regression measurement system can be realized using ultrasound sensors [27], miniature resistive regressions, and ablation sensor (MIRRAS) [27], or additively manufactured solid fuels with the fuel regression measurement function [28]. Here, the measurement errors and the valve control were not considered in the calculation of the O/F-controlled cases, to acquire their ideal performance. The delay time of the thrust and O/F control was assumed to be the same as the timestep of the calculation: 10 [ms]. This flight simulation did not consider the additional mass to control the effective geometric swirl number due to the complexity of its sizing. However, the resultant residual propellant mass will infer the scale of acceptable additional mass.

C. **Simulated Cases**

Flight simulations of three scales of rockets, corresponding to the Japanese sounding rocket series S-520 [29], S-310, and S-210 [30], were performed for this study. Table 1 and Fig. 9 summarize the dimensions of the rockets simulated and their definitions, respectively. The dimensions of the rockets were analytically calculated under the constraints of the physical properties of the propellants. The design conditions assumed were the physical properties of the propellants, rocket and propellant mass, nozzle expansion ratio, the maximum oxidizer mass flux in the fuel port, initial fuel port-to-throat area ratio, initial geometric swirl number for O/F-controlled rockets, the initial thrust-

to-weight ratio of the propulsion subsystem, and the specific impulse used only when scaling the initial mass flow rate. This specific impulse was 280 [s], which corresponds to the sea level specific impulse at a chamber pressure of 3 [MPa] and O/F of 2.0, was used only for the scaling of the initial thrust-to-weight ratio of the propulsion system at liftoff. For this investigation, the propellant O/F was selected to give the largest ΔV in each scale for the median fuel regression behavior [9]. The O/F-uncontrolled rockets had the same dimensions as the O/F-controlled rockets. It should be noted that for the O/F-uncontrolled rockets, the geometric swirl number was adjusted so that the fuel and oxidizer were spent simultaneously at engine cut-off under the median fuel regression behavior. For comparison purposes in the systematic error cases, cases where the propellant O/F was shifted slightly in the fuel-rich direction were also calculated to improve the worst performance of the O/F-uncontrolled rockets [6]. Their propellant O/F were selected so that the oxidizer residual mass for the $+3\sigma$ case is the same with the fuel residual mass for -3σ case. These design parameters are also summarized in Table 1 with the initial mass and mass fractions of the rockets.

For the flight simulations with the systematic errors in the fuel regression behavior, the 6 cases with constant systematic errors corresponding to $\pm 1\sigma$, $\pm 2\sigma$, and $\pm 3\sigma$ were calculated for each scale of the O/F-controlled and –uncontrolled rockets using Eq. (13). For the cases with random errors, the actual regression rate is randomly determined by the probability density function Eq. (14) at each time step. The flight simulations were repeated 3008 times for each scale of the O/F-controlled and –uncontrolled rockets to collect the statistics of flight performance. The number of trials is based on the probability of the appearance of $\pm 3\sigma$, 0.27%. At least 8 cases corresponding to $\pm 3\sigma$ are expected to appear out of the 3008 cases.

V. Results and Discussion

A. Systematic Error Cases

Figure 10 and Table 2 show the highest altitudes, ΔV, the averaged specific impulse, and residual propellant mass versus the scale of the systematic error for both the O/F-controlled and –uncontrolled rockets. There were significant performance gaps between the O/F-controlled and -uncontrolled rockets, especially under the presence of systematic errors. For the nominal fuel regression ($\sigma = 0$), the performance increases ranged 4.7-7.1% in the highest altitude, 1.7-2.1% in ΔV, and 2.0-2.4% in the averaged specific impulse, respectively. As stated in Ref. [9], these small performance increases of the O/F-controlled rocket should be cancelled out by the increase of the structural mass of a more complex oxidizer feed system, because this result suggests that, for the rocket mass budget, the acceptable mass

for the O/F-controlled rockets correspond to 1.0-1.3% of the initial mass when roughly estimating with the first-order approximation of the Tsiolkovsky equation.

However, when considering constant systematic errors in the fuel regression rate equation, the O/F-controlled rockets performed considerably better than the O/F-uncontrolled rockets. The O/F-controlled rockets maintained the best flight performance in all but a few cases. We should note that the three cases with negative systematic errors resulted in slightly higher altitudes than those in the nominal regression behavior by less than approximately 0.39% probably because thrust control or propellant O/F, which depends on chamber pressure and nozzle expansion ratio or thrust control, was not strictly optimum. The ΔV for the O/F-controlled rockets followed this trend with a small discrepancy of less than 0.34%. Although these simulations were not carried out with the optimum time-history of O/F and throttling, it is remarkable that the O/F-controlled rockets maintained their flight performance even under the presence of systematic errors. The O/F-uncontrolled hybrid rockets did not maintain their best flight performance. Both the highest altitude and specific impulse linearly decreased with the size of the errors. The worst performance in these simulations was for $+3\sigma$ where the highest altitude and ΔV were 218 [km] and 2.66 [km/s] for the 2100 [kg] rocket, respectively, corresponding to 10.6% and 4.73% lower performance than for the nominal case. The ΔV for the O/F-uncontrolled rocket with the $+3\sigma$ error was 5.86% lower than that of the worst case of O/F-controlled rocket. For the O/F-uncontrolled rocket, the residual mass increased with increasing fuel regression error whereas the negative error in the fuel regression increased the averaged specific impulse similarly to the O/F-controlled rocket. The residual propellant mass for the positive errors was approximately two times larger than for that of the negative errors because the propellant O/F was 1.8 to 1.9. Fuel-rich cases were also calculated for the O/F-uncontrolled rockets to decrease the oxidizer residual mass and improve the worst performance for $+3\sigma$ [6]. The propellant O/Fs shifted to 1.74, 1.83, and 1.83, respectively so that the residual mass is equal for $\pm 3\sigma$. For all scales, these fuel-rich motor designs shifted the best performance to the case with the $+1\sigma$ error and improved the highest altitudes and acceleration for the $+3\sigma$ case. However, even the best performance for the $+1\sigma$ cases did not reach that of the initial motor design, and the $+3\sigma$ cases still had the worst performance in the $\pm 3\sigma$ uncertainty probably because of the smaller specific impulse for $+3\sigma$ cases. These improved worst performance cases correspond to those of the initial designs between $+2\sigma$ and $+3\sigma$. The O/F-controlled rockets still had 4.93 to 6.69% greater ΔV and 12.6 to 20.4% higher altitude, even when compared with the fuel-rich motor design. The residual propellant mass ranged between 0.99-1.18% of the initial mass for the $\pm 3\sigma$ cases. Therefore, when combining the specific impulse loss for the nominal fuel regression with the

residual propellant of the $\pm 3\sigma$ systematic uncertainty, O/F control improves performance and allows us to omit quality control of fuel regression behavior if its function can be added to the closed-loop thrust control system with less than 2.18 to 2.29 % of the initial mass.

The reason for the large performance drop in ΔV is easily explained by the first-order approximation of the Tsiolkovsky rocket equation, assuming specific impulse and final mass as the only independent variables. The normalized ΔV drop, $d(\Delta V)/\Delta V$, is approximated by those of final mass m_f and specific impulse I_{sp}:

$$\frac{d(\Delta V)}{\Delta V} \sim \frac{d\overline{I_{sp}}}{\overline{I_{sp}}} - \frac{1}{\ln m_i/m_f}\frac{dm_f}{m_f} + \frac{\mathcal{O}\left(\delta^2(\overline{I_{sp}})+\delta^2(m_f)\right)}{\Delta V} \sim \frac{d\overline{I_{sp}}}{\overline{I_{sp}}} - \frac{1}{\ln m_i/m_f}\frac{m_p}{m_f}x \tag{17}$$

where x is residual propellant mass to initial propellant mass ratio. The approximations agreed well with those of flight simulations within 0.271-point errors, therefore, Eq. (17) enabled us to roughly estimate the proportions of the performance drop of the O/F-uncontrolled rockets. Figure 11 shows the share breakdown in the total performance drop for all scales of rockets, compared to the cases without the fuel regression error. For the 233 [kg] rockets with $+3\sigma$ error, the performance drop due to specific impulse was larger than that of the other large scales, so that the residual propellant mass contributed to 60 % of the ΔV drop. However, the decrease in performance seems to become less sensitive to the scale for the hybrid rockets larger than 700 [kg], therefore, the contribution of the residual propellant became more dominant and reached approximately 63% for the larger two scales. The residual mass problem causes one of the most dominant factors in the performance drop of this sounding rocket flight simulation, but it should have a 10 times greater impact on satellite launchers. This is because the term $\left(\ln m_i/m_f\right)^{-1} m_p/m_f$ appearing in Eq. (17) is calculated to be 85.4 for the typical propellant mass fraction of satellite launchers of 90%, whereas this parameter was 7.41 for the 71.4% propellant mass fraction of the rockets simulated in this paper. Therefore, identifying and stabilizing the fuel regression behavior is critical for the practical use of hybrid rockets, especially for systems with a high propellant mass fraction.

The estimation of the proportion of performance losses due to specific impulse losses was also carried out with the methodology used in the benchmark of the O/F-controlled and –uncontrolled hybrid rockets under the nominal fuel regression behavior, as shown in Fig. 12. Note that the enthalpy shift loss is the value compared to the ideal time-averaged specific impulse of the O/F-controlled rockets with 100 c* efficiency and without nozzle throat erosion or fuel regression errors. c* efficiency was the most dominant in the specific impulse drop among enthalpy shift, c* efficiency, nozzle throat erosion also under the presence of fuel regression errors, and this trend was observed also

under the nominal fuel regression behavior [9]. These shares and the total specific impulse drop had slight sensitivity to the fuel regression errors. This breakdown of ΔV and specific impulse drops revealed that, in the presence of systematic fuel regression errors, the residual propellant problem leads to a significant degradation in the flight performance of hybrid rockets, even for the propellant mass fraction of approximately 70%.

B. Random Error Cases

Figure 13 shows the typical time-traces of O/F-controlled and –uncontrolled rockets in the 3008 flight simulations with random errors in fuel regression behavior. Here, O/F is randomly distributed around its nominal time-trace according to the designated probability distribution during the powered flight. The random O/F shifts tended to decrease the specific impulse, especially during deep throttling for the O/F-uncontrolled rockets because O/F shifted in the more fuel-rich direction.

Both types slightly decreased the flight performance, compared to that for the nominal fuel regression, but the variance of random errors in the fuel regression directly lowered the accuracy of the performance of the O/F-uncontrolled rockets. Figure 14 shows the histograms of the distributions of the highest altitudes, ΔV, specific impulse, and residual propellant mass in the 3008 flight simulations. The statistically important characteristics of the results are summarized in Table 3. The averaged values of the highest altitudes and ΔV for the total mass of the 2100 [kg] rockets were 253 [km] and 2.82 [km/s], respectively, for the O/F-controlled rocket, compared to 241 [km] and 2.78 [km/s] for the O/F-uncontrolled rocket. The ΔV losses due to random errors were -0.784% and -0.823% of the nominal value for the O/F-controlled and O/F-uncontrolled rockets, respectively. The averaged performance drops and their standard deviations had a slight dependency on the scale of rockets, but this effect was negligible small with a 1% margin of ΔV for all scales. The differences between the best and the averaged performance of the O/F-uncontrolled rockets spanned from -1.37% in highest altitude and -0.37% in ΔV for the 233 [kg] rocket to -0.823% and -0.358% for the 2100 [kg] rocket.

There were relatively large variances in the performance of the O/F-uncontrolled rockets whereas the O/F-controlled rockets succeeded in stabilizing the flight performance. The standard deviations of the highest altitudes and ΔV for the O/F-uncontrolled rockets were 1.24[km] and 5.93[m/s] whereas those for the O/F-controlled rockets were 0.181 [km] and 0.820 [m/s], respectively. This result says that the O/F-controlled rockets had at least 6.61 times the accuracy of acceleration of all scales of rockets simulated. The standard deviation normalized by the performance factors for the O/F-uncontrolled rockets followed the trend of the averaged performance: 0.727% in the highest altitude

and 0.257% in ΔV for the 233[kg] rocket; 0.515% in the highest altitude and 0.129% in ΔV for 2100 [kg] rocket, respectively. However, we should note that the standard deviation of ΔV corresponds to at most 0.257% of the total ΔV, even for O/F-uncontrolled rockets, so that this error seems to be acceptable within a ΔV margin.

The residual propellant mass took the form of a power-law distribution. A few flights with a remarkable performance drop were found for the O/F-uncontrolled rockets. 1 to 2 of 3008 flights caused residual propellant mass larger than 0.5% of the initial propellant mass, leading to performance decreases between 1.88 and 5.39% in ΔV. The residual propellant mass should be taken into account to explain the performance drop not only with the specific impulse drop also under the random error conditions. Using Eq. (17), it was found that approximately 42.0 to 59.9% of the ΔV drops were caused by the residual propellant mass without considering the specific impulse loss of the O/F-controlled cases. The decrease in the proportions of performance loss due to residual propellant mass compared to the systematic error cases are because 1σ of random regression error is larger than that of the systematic constant regression error, but the instantaneous residual propellant mass is compensated for by the randomness of the error.

These statistical analyses revealed that, although the O/F-uncontrolled rockets have a good averaged (or expected) performance even compared to the O/F-controlled rockets, there are a relatively large performance drops in the worst cases corresponding to $\pm 3\sigma$, resulting almost equally from residual propellant mass and specific impulse drops. As a result, under the presence of random errors in fuel regression, the advantage of O/F-controlled hybrid rockets have a more stable performance and a worst case ΔV that is 4.06 to 4.49% higher than the O/F-uncontrolled hybrid rockets. Moreover, it is also important to recognize the difference in the magnitude of the performance drops due to systematic errors and random errors in fuel regression behaviors. The suitable countermeasure against various O/F shifts may depend on the contributions of these respective factors to the performance drops.

VI. Conclusions

This paper discusses the sources of O/F shifts, and the paths through which they affect the propulsive and flight performance of hybrid rockets. Flight simulations of vertically launched single-stage sounding rockets were performed under systematic and random error models based on experimental results to evaluate the performance of O/F-controlled and O/F-uncontrolled hybrid rockets.

The sources of O/F shifts originating in the fuel regression behavior were classified in detail. One of the sources is the non-linear sensitivity of regression behavior to oxidizer mass flux, which causes O/F shifts according to the

median (nominal) regression rate equations. The other source is the uncertainty of the fuel regression deviations from the median fuel regression behavior. The latter source is classified into two types: 1) the uncertainty of the median fuel regression; 2) random errors according to a probability distribution. The paths of O/F shifts through which propulsive and flight performance are affected were also classified, as: 1) shifts of the thermodynamic state of the product gases, such as enthalpy and ratio of specific heat; 2) c* efficiency; 3) nozzle throat erosion made of graphite or other carbon-based materials; 4) residual propellant mass. The residual propellant mass does not affect the engine performance but does directly affect ΔV. The residual propellant is caused by the uncertainties of fuel regression behavior as well as by deviations in thrust from the initially planned thrust curve.

The performance increase of O/F-controlled hybrid rockets was evaluated by simulating vertical launches of three scales of O/F-controlled and –uncontrolled single-stage hybrid sounding rockets. The first set of simulations was that of launches under fixed systematic errors in the fuel regression behavior. Under the $+3\sigma$ error of fuel regression, the O/F-controlled rockets maintained their median performance, and outperformed the O/F-uncontrolled rockets by 4.93 to 6.69% in ΔV. This performance increase was observed even when comparisons were held for fuel-rich motor designs aiming to reduce the oxidizer residual mass for $+3\sigma$ cases. The breakdown of the performance drops of the O/F-uncontrolled hybrid rockets revealed that more than 60% of the total ΔV loss was due to the residual propellant mass over all three scales of rockets and systematic errors. The residual propellant masses ranged from 0.99-1.18% of the initial mass for fuel-rich designs with $\pm 3\sigma$ errors. Therefore, when combining the specific impulse loss for the nominal fuel regression with the residual propellant of the $\pm 3\sigma$ systematic uncertainty, O/F control improves performance of the rocket if its function can be added to the closed-loop thrust control system with less than 2.18-2.29 % of the initial mass. In this study, a propellant mass fraction of 71.4% was implemented, implying that the residual propellant mass will be a critical problem for the practical use of hybrid rockets as satellite launchers, which typically require a propellant mass fraction of more than 90%. The proportions of performance loss due to decreases in specific impulse were hardly affected by systematic errors. The second set of flight simulations was conducted under random errors in the fuel regression behavior for each scale of O/F-controlled and –uncontrolled type rockets. The averaged flight performance of both types of hybrid rockets slightly decreased from their nominal performance, but there were considerable gaps in the accuracy of performance and the worst case performances of both types. The O/F-controlled rockets succeeded in eliminating most of the residual propellants and decreasing the standard deviations of the flight performance. On the other hand, although the O/F-uncontrolled rockets exhibited the expected

performance under nominal fuel regression, the standard deviation of ΔV was more than 6.61 times larger than that of the O/F-controlled type. O/F-control considerably improved the performance of the worst cases by upwards of 4.49% in ΔV. Unlike the results of the fixed systematic fuel regression errors, the residual propellant mass had 42.0 to 59.9 % of the proportion of total ΔV drop. Relatively large instantaneous O/F shifts and small residual mass can explain the difference of the proportions of ΔV loss from that under the fixed systematic fuel regression errors. Since all simulation results were obtained for rockets with a 71.4% propellant mass fraction, it can be said that the contribution of the residual propellant mass to the ΔV loss will be larger in rockets with larger propellant mass fractions.

In conclusion, this paper clarifies that O/F-controlled hybrid rocket propulsion considerably improves flight performance of single-stage hybrid sounding rockets by 6.69% and 4.49 % in ΔV under $\pm 3\sigma$ systematic and random errors, respectively. Therefore, as well as the identification of the fuel regression behavior, techniques to eliminate O/F shifts and residual propellants should play an important role in hybrid rocket development, especially for hybrid rockets with large propellant mass fractions.

Acknowledgments

This work was financially supported by JSPS KAKENHI 15J08028, 16H04594, and 18K13926, the Foundation for the Promotion of the Industrial Explosives Technology, and the Hattori Hokokai Foundation. This research was supported by the Hybrid Rocket Research Working Group (HRRWG) of the Institute of Space and Astronautical Science, Japan Aerospace Exploration Agency. The authors thank members of HRRWG for their helpful discussion.

References

[1] Ordahl, D. D., "Recent Developments and Current Status of Hybrid Rocket Propulsion," *Journal of Spacecraft and Rockets*, Vol. 2, No. 6, Nov. 1965, pp. 923–926.
doi: 10.2514/3.28315

[2] Waidmann, W., "Thrust Modulation in Hybrid Rocket Engines," *Journal of Propulsion and Power*, Vol. 4, No. 5, Sept.-Oct., 1988, pp. 421–427.
doi: 10.2514/3.23083

[3] Humble, R. W., Henry, G. N., and Larson, W. J., *Space Propulsion Analysis and Design*, McGraw-Hill, New York, 1995, Chap. 7.
doi: 10.1036/0070313202

[4] Karabeyoglu, A. M., and Evans, B. J., "'O/F Shift' in Hybrid Rockets," *50th AIAA/ASME/SAE/ASEE Joint Propulsion Conference & Exhibit*, AIAA, Cleveland, Ohio, 2014, AIAA 2014-3851.
doi: 10.2514/6.2014-3851

[5] Barato, F., Grosse, and M., Bettella, A., "Hybrid Rocket Residuals - An Overlooked Topic," *50th AIAA/ASME/SAE/ASEE Joint Propulsion Conference & Exhibit*, AIAA, Cleveland, Ohio, 2014, AIAA 2014-3753.
doi: 10.2514/6.2014-3 753

[6] Casalino, L., and Pastrone, D., "A Straightforward Approach for Robust Design of Hybrid Rocket Engine Upper Stage," *51st AIAA/SAE/ASEE Joint Propulsion Conference*, AIAA, Orlando, Florida, 2015, AIAA 2015-4202.
doi: 10.2514/6.2015-4202

[7] Casalino, L., Masseni, F., and Pastrone, D., "Uncertainty Analysis and Robust Design for a Hybrid Rocket Upper Stage," *Journal of Spacecraft and Rockets*, Vol. 56, No. 5, Sep. 2019, pp. 1–8.
doi: 10.2514/1.A34422

[8] Casalino, L., Pastrone, D., and Masseni, F., "Robust Design of Hybrid Rocket Engine for Small Satellite Launchers," *AIAA Propulsion and Energy 2019 Forum*, AIAA, Indianapolis, Indiana, 2019, AIAA 2019-4096.
doi: 10.2514/6.2019-4096

[9] Ozawa, K., and Shimada, T., "Performance of Mixture-Ratio-Controlled Hybrid Rockets for Nominal Fuel Regression," *Journal of Propulsion and Power*, Vol. 36, No. 3, Mar. 2020, pp. 400–414.

[10] Sutton, G, P., and Biblarz O., *Rocket Propulsion Elements*, 7th ed., John Wiley & Sons, Inc., Hoboken, 2001, Chap. 10.

[11] Ozawa, K., Kitagawa, K., Aso, S., and Shimada, T., "Hybrid Rocket Firing Experiments at Various Axial–Tangential Oxidizer-Flow-Rate Ratios," *Journal of Propulsion and Power*, Vol. 35, No. 1, Jan. 2019, pp. 94–108.
doi: 10.2514/1.B36889

[12] Shimada, T., Yuasa, S., Nagata, H., Aso, S., Nakagawa, I., Sawada, K., Hori, K., Kanazaki, M., Chiba, K., Sakurai, T., Morita, T., Kitagawa, K., Wada, Y., Nakata, D., Motoe, M., Funami, Y., Ozawa, K., Usuki, T., "Hybrid Propulsion Technology Development in Japan for Economic Space Launch," edited by L., De Luca, T., Shimada, V., P., Sinditskii, and M. Calabro, *Chemical Rocket Propulsion: A Comprehensive Survey of Energetic Materials*, Springer Aerospace Technology, Springer International Publishing, Cham, Switzerland, 2017, pp. 545-575.
doi: 10.1007/978-3-319-27748-6

[13] Bianchi, D., and Nasuti, F., "Numerical Analysis of Nozzle Material Thermochemical Erosion in Hybrid Rocket Engines," *Journal of Propulsion and Power*, Vol. 29, No. 3, 2013, pp. 547–558.
doi: 10.2514/1.B34813

[14] Shinohara, K., and Nakagawa, I., "Regression Rate Characteristics of Paraffin-based Fuel under Swirled Oxidizer Flow," *48th AIAA/ASME/SAE/ASEE Joint Propulsion Conference & Exhibit*, AIAA, Atlanta, Georgia, 2012, AIAA 2012-4104.
doi: 10.2514/6.2012-4104

[15] Saito, D., Yuasa, S., Hirata, K., Sakurai, T., and Shiraishi, N., "Combustion Characteristics of Paraffin-Fueled Swirling Oxidizer-Flow-Type Hybrid Rocket Engines," *48th AIAA/ASME/SAE/ASEE Joint Propulsion Conference & Exhibit*, AIAA, Atlanta, Georgia, 2012, AIAA 2012-3904.
doi: 10.2514/6.2012-3904

[16] Karabeyoglu, M., A., Zilliac, G., Cantwell, B., J., Zilwa, S., D., and Castellucci, P., "Scale-up Tests of High Regression Rate Liquefying Hybrid Rocket Fuels," *Journal of Propulsion and Power*, Vol. 20, No. 6, Nov.-Dec., 2004, pp. 1037-1045.
doi: 10.2514/1.3340

[17] Ross, S. M., *Introduction to Probability and Statistics for Engineers and Scientists*, 4th ed., Elsevier Academic Press, Massachusetts, 2009, Chap. 9.

[18] Ross, S. M., *Introduction to Probability and Statistics for Engineers and Scientists*, 4th ed., Elsevier Academic Press, Massachusetts, 2009, Chap. 5.

[19] Gordon, S., and McBride, J. B., "Computer Program for Calculation of Complex Chemical Equilibrium Compositions and Applications," NASA Reference Publication 1311, 1994.

[20] McCabe W. L., and Smith, J. C., *Unit Operations of Chemical Engineering*, 3rd ed., McGraw-Hill Education, New York, 1976, Chap. 4.

[21] Kamps, L., Saito Y., Kawabata, R., Wakita, M., Totani, T., Takahashi, Y., and Nagata, H. "Method for Determining Nozzle-Throat-Erosion History in Hybrid Rockets," *Journal of Propulsion and Power*, Vol. 33, No. 6, Nov. 2017, pp. 1369-1377.
doi: 10.2514/1.B36390

[22] Huzel, D. K., and Huang, D. H. (ed.), *Modern Engineering for Design of Liquid-Propellant Rocket Engines*, AIAA, Washington DC, 1992, Chap. 4.
doi: 5.9781600866197.0067.0134

[23] Saito, D., Yuasa, D., Sakurai, T., Shiraishi, N., "Effects of Post Combustion Chamber on Combustion Characteristics of Paraffin-Fueled Swirling Oxidizer-Flow-Type Hybrid Rocket Engine," *Space Transportation Symposium FY2012*, Institute of Space and Astronautical Science, Japan Aerospace Exploration Agency, Sagamihara, Kanagawa, Japan, 2013, STCP-2012-075. (Japanese)

[24] Ishiguro, T., Shinohara, K., Sakio, K., and Nakagawa I., "Combustion Efficiency of Paraffin-based Hybrid Rockets," *47th AIAA/ASME/SAE/ASEE Joint Propulsion Conference & Exhibit*, AIAA, San Diego, California, 2011, AIAA 2011-5679.
doi: 10.2514/6.2011-5679

[25] Ben-Asher, J. Z., *Optimal Control Theory with Aerospace Applications*, AIAA, Reston, 2010, Chaps. 4 and 9.
doi: 10.2514/4.867347

[26] Narsai, P., Venkataraman, K., Stober, K., J., and Cantwell, B., J., "Measuring Nozzle Erosion in a Hybrid Rocket Motor with Ultrasound," *52nd AIAA/SAE/ASEE Joint Propulsion Conference*, AIAA, Salt Lake City, Utah, 2016, AIAA 2016-4753.
doi: 10.2514/6.2016-4753

[27] Chiaverini, M. J., and Kuo, K. K., *Fundamentals of Hybrid Rocket Combustion and Propulsion*, AIAA, Reston, 2007, Chap. 4.

[28] Ozawa, K., Wang, H., Yoshino, T., and Tsuboi, N., "Real-time Regression Rate Measurement of an Additive-manufactured Functional Hybrid Rocket Fuel," *70th International Astronautical Congress*, IAF, Washington D.C., 2019, IAC-19,C4,2,9,x53606.

[29] Matsuno, H., Kohno, M., Onoda, J., Kawashima, T., Murakami, T., and Onojima, N., "Development of the S-520 Single Stage Sounding Rocket," *Acta Astronautica*, Vol. 9, No. 10, 1982, pp. 631–635.
doi: 10.1016/0094-5765(82)90107-2

[30] Hirasawa, T., "Sounding Rocket Experiment at Syowa Station, Antarctica," *The Journal of Space Technology and Science*, Vol. 7, No. 1, 1991, pp. 1_9-1_17.
doi: 10.11230/jsts.7.1_9

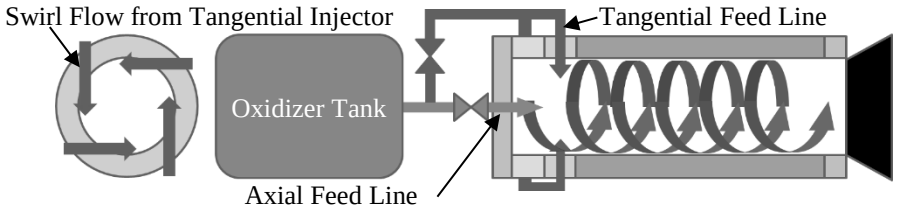

Fig. 1 Concept of Altering-intensity Swirling-Oxidizer-Flow-Type (A-SOFT) hybrid rocket engines [11].

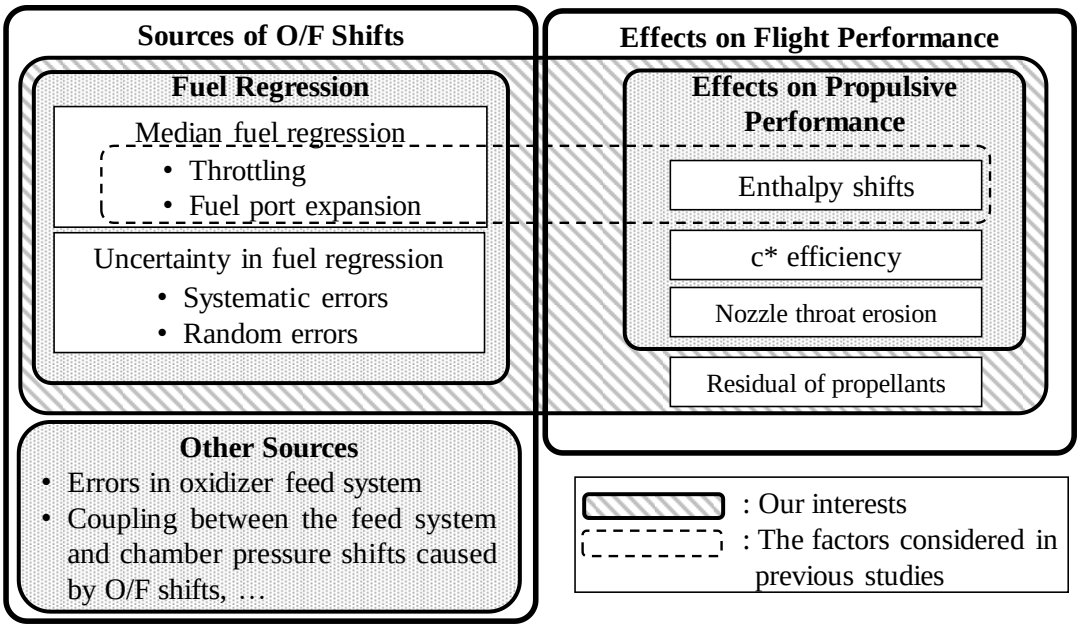

Fig. 2 Sources of O/F shifts and paths via which O/F shifts affect flight performance.

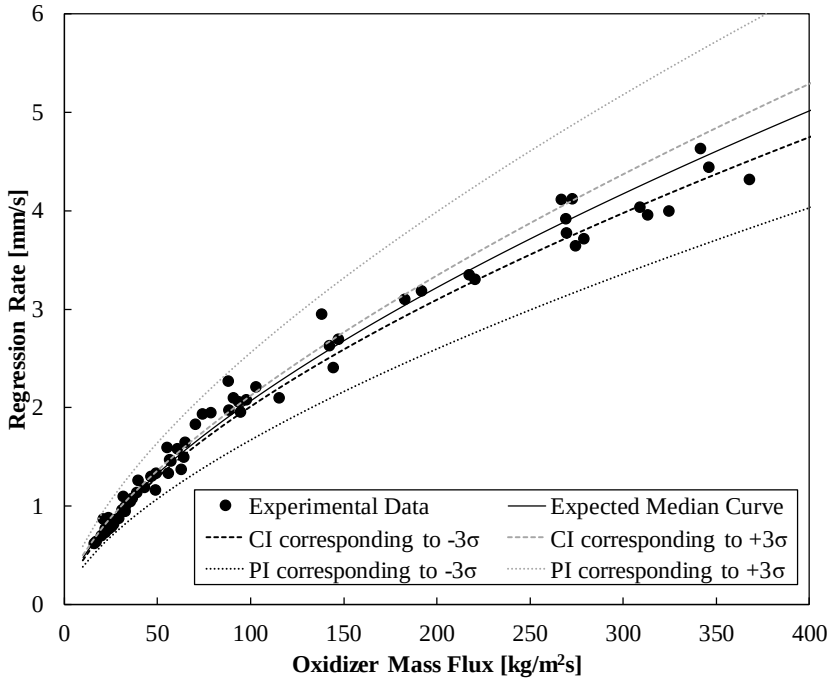

Fig. 3 Multiple linear regression analysis of regression rate behavior of axial hybrids using paraffin wax and GOX with its confidence interval and prediction interval.

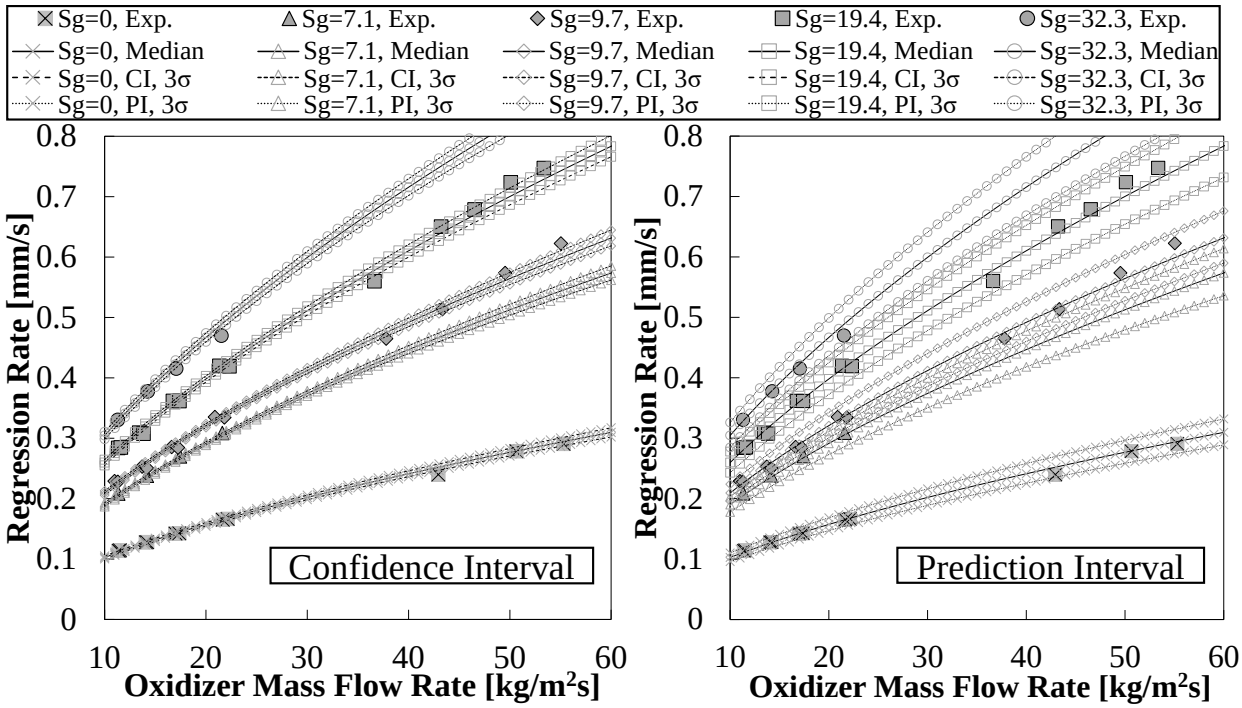

Figure 4. Multiple linear regression analysis of the regression rate behavior of SOFTs using PMMA and GOX with its 3σ boundaries of confidence and prediction intervals.

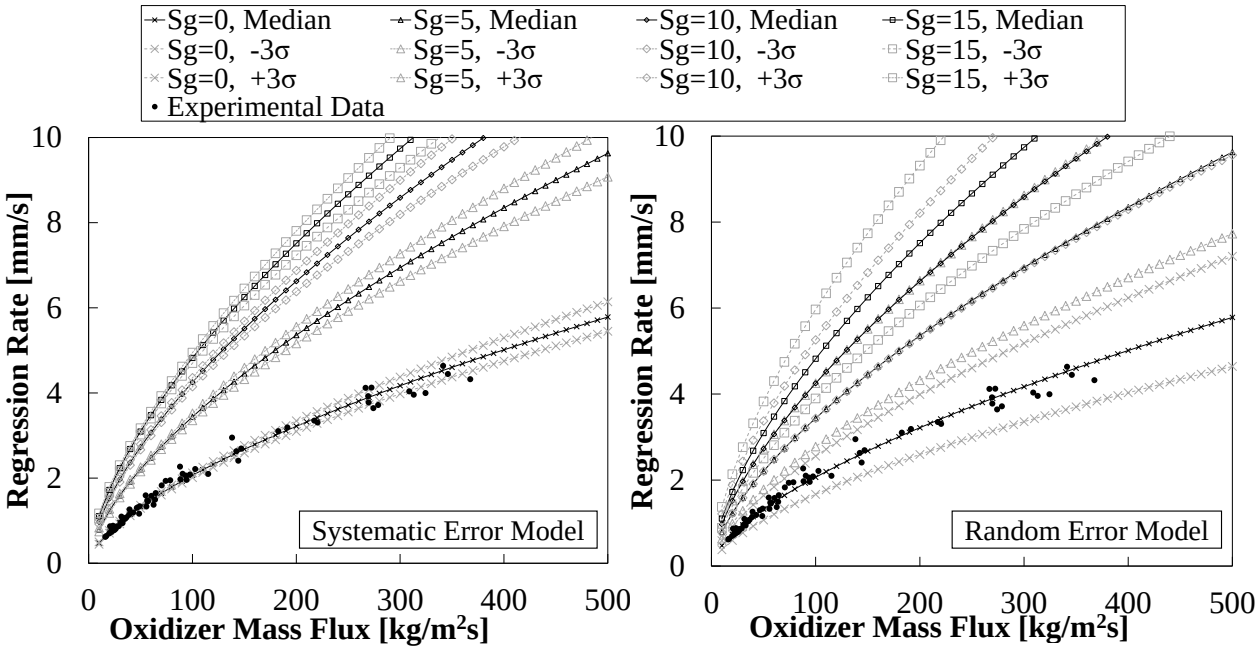

Figure 5. Systematic and Random Error models with their 3σ boundaries.

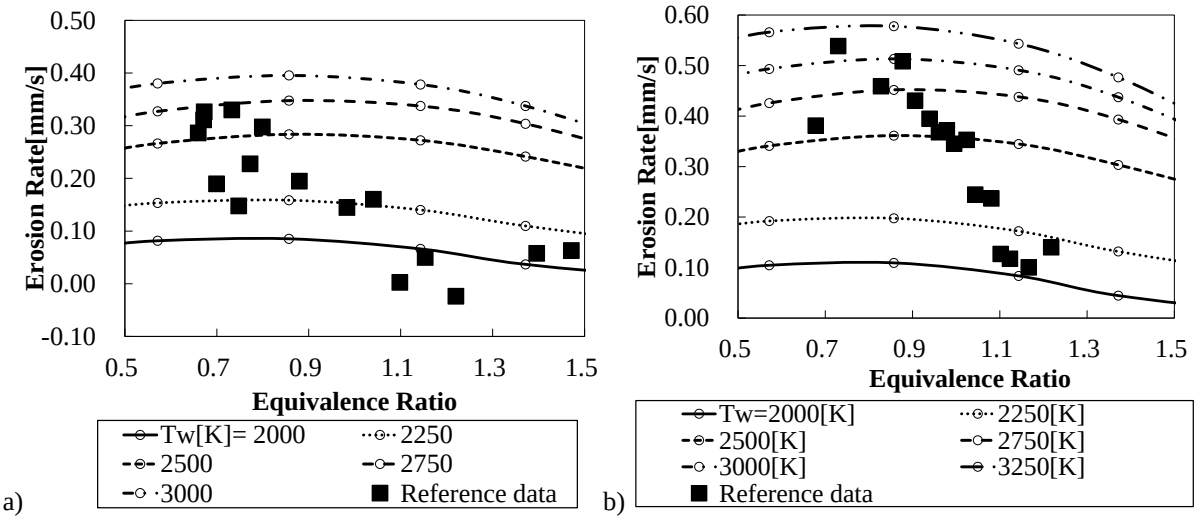

Fig. 6 Comparison of the throat erosion model with the experimental data [21] a) Test 1 and b) Test 4.

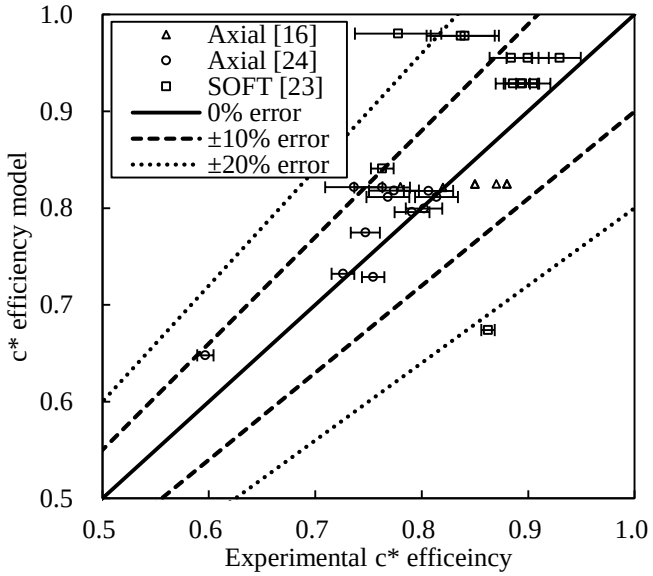

Fig. 7 Comparison of the c* efficiency model with the experimental data.

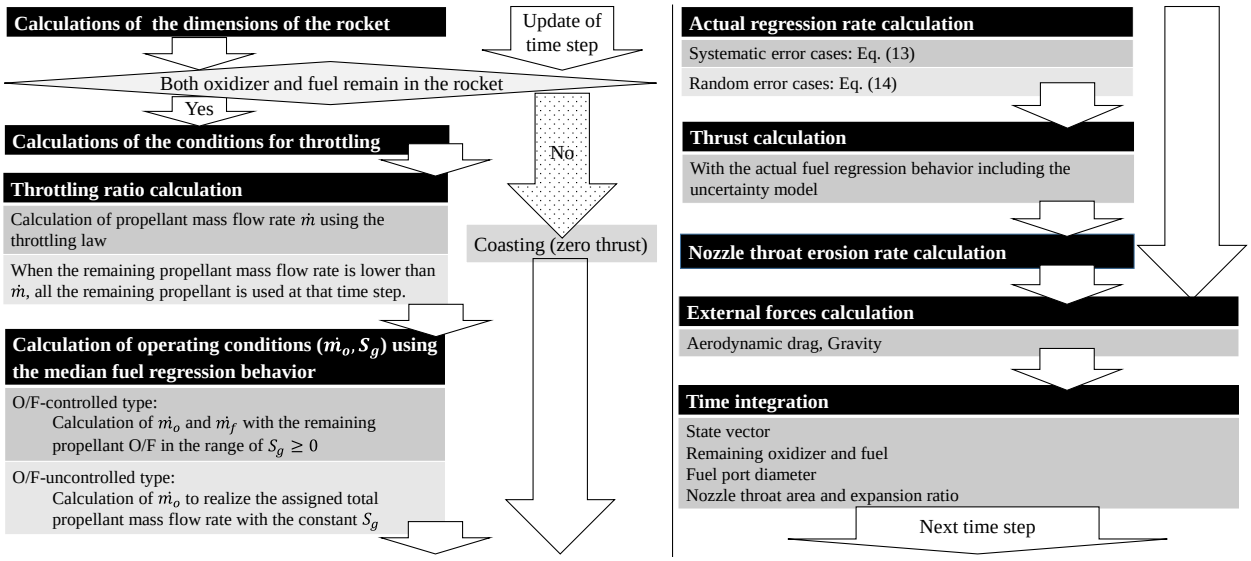

Fig. 8 Block diagram of the flight simulation program.

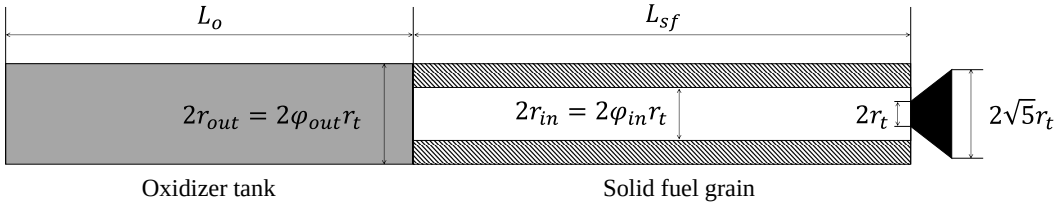

Fig. 9 Configuration of the propulsive subsystem of a hybrid sounding rocket.

Table 1 Specifications of sounding hybrid rockets.

Assumed Design Conditions	Initial Mass, kg	233	700	2100
	Propellant Mass, kg	166.5	500.25	1500
	Fuel Density, kg/m3		760	
	Oxidizer Density, kg/m^3		1140	
	Nozzle Expansion Ratio		5.0	
	Initial Fuel Port-to-Throat Area Ratio		3.0	
	Initial Thrust-to-Weight Ratio of the Propulsion Subsystem		10.0	
	Initial Geometric Swirl Number for the O/F-controlled Type		6.0	
	Maximum Oxidizer Mass Flux, kg/m^{2}s		350	
Design Parameters Derived from the Constraints and Nominal Performance Evaluation	Propellant O/F	1.8	1.9	1.9
	Initial Fuel Port Diameter, m	0.140	0.244	0.423
	Outer Diameter, m	0.331	0.467	0.673
	Solid Fuel Grain Length, m	1.10	1.83	3.16
	Oxidizer Tank Length, m	1.09	1.68	2.43
	Aspect Ratio of Propulsion Subsystem	6.60	7.50	8.30
	Geometric Swirl Number for the O/F-uncontrolled Type	3.65	3.64	3.69
	Propellant O/F for Fuel-rich Design	1.74	1.83	1.83
Resultant Values (O/F-controlled)	Nominal Initial Chamber Pressure, MPa	2.98	2.95	2.95
	Nominal Minimum Oxidizer Mass Flux, kg/m^{2}s	15.0	21.2	34.2
	Nominal Minimum Oxidizer Mass Flow Rate, kg/s	0.881	2.55	9.07
Resultant Values (O/F-uncontrolled)	Nominal Minimum Oxidizer Chamber Pressure, MPa	2.87	2.81	2.82
	Nominal Minimum Oxidizer Mass Flux, kg/m^{2}s	13.4	18.8	28.0
	Nominal Minimum Oxidizer Mass Flow Rate, kg/s	0.785	2.28	7.47

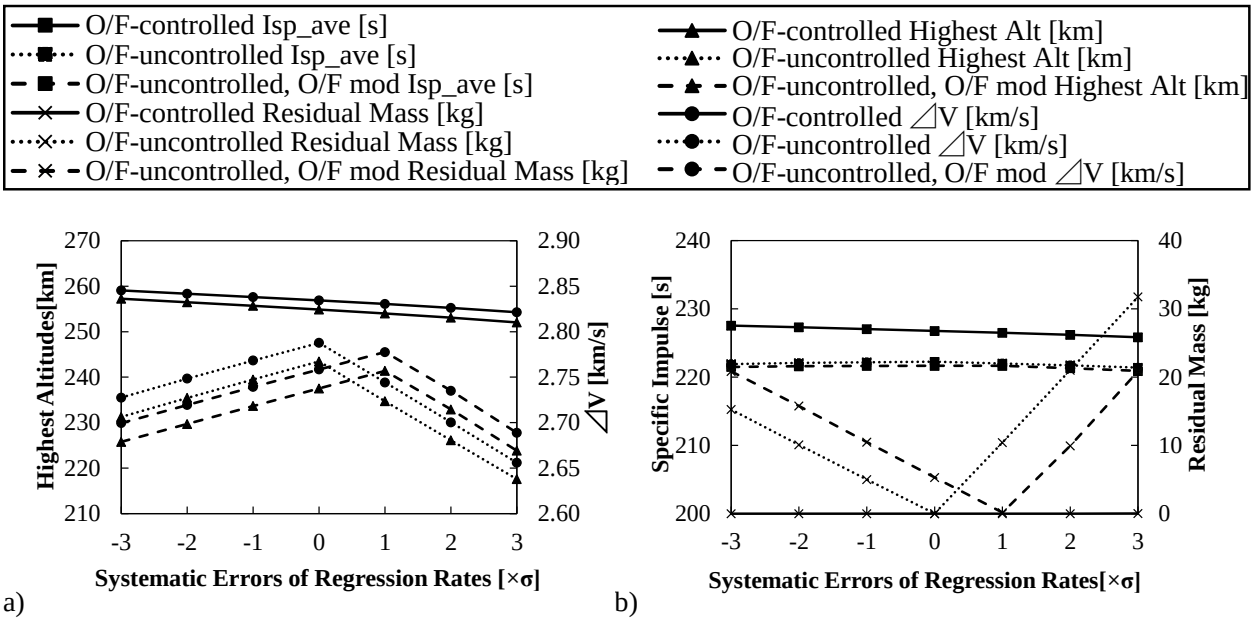

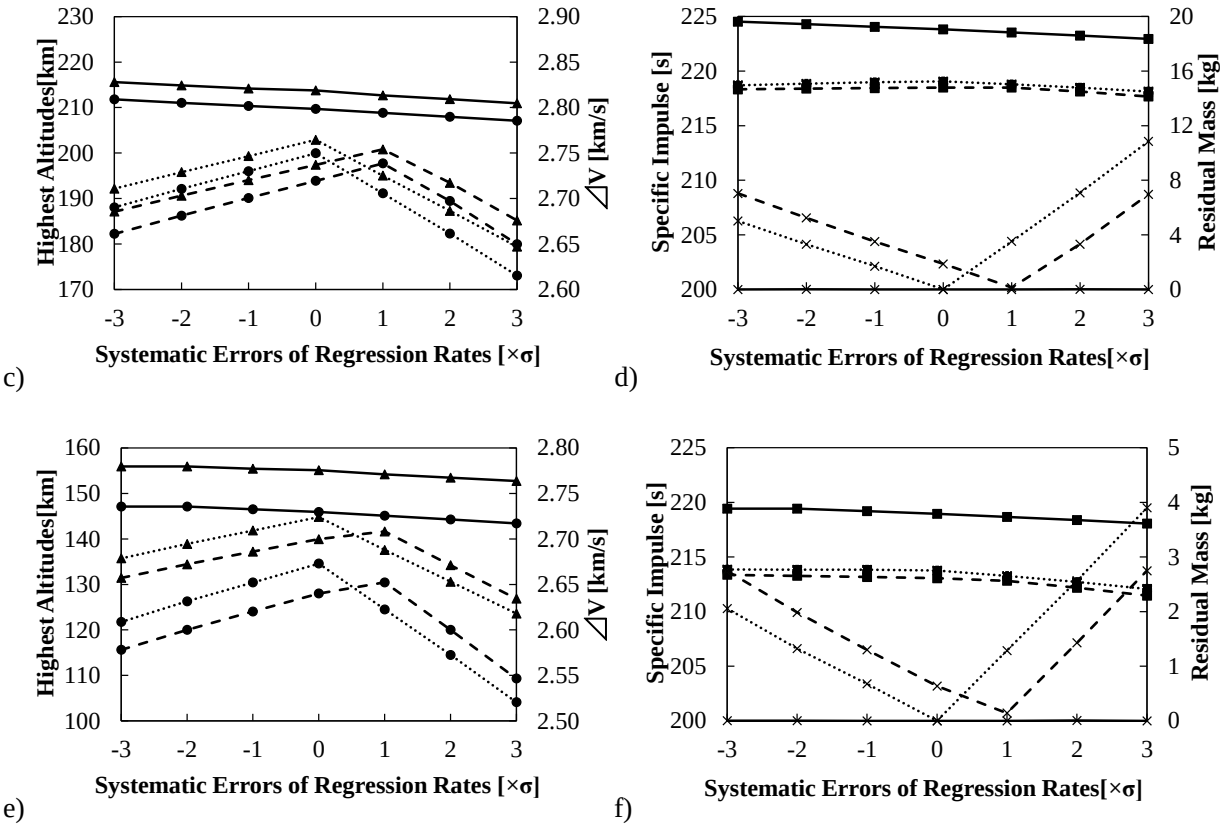

Fig. 10 Summary of flight performance under the fuel regression behavior with systematic errors: a) and b) initial mass of 2100 [kg]; c) and d) 700 [kg]; e) and f) 233 [kg].

Table 2 Results of the flight simulations under systematic errors

		Scale of Error	-3σ	-2σ	-1σ	0	$+1\sigma$	$+2\sigma$	$+3\sigma$
O/F-controlled	233 kg	Highest Altitude, km	156	156	155	155	154	153	153
		ΔV, km/s	2.74	2.74	2.73	2.73	2.73	2.72	2.72
		$\overline{I_{sp}}$, s	219	219	219	219	219	218	218
		Residual Propellant Mass, kg	0.00	0.00	0.00	0.00	0.00	0.00	0.00
	700 kg	Highest Altitude, km	216	215	214	214	213	212	211
		ΔV, km/s	2.81	2.81	2.80	2.80	2.79	2.79	2.79
		$\overline{I_{sp}}$, s	225	224	224	224	224	223	223
		Residual Propellant Mass, kg	0.00	0.01	0.00	0.00	0.00	0.01	0.00
	2100 kg	Highest Altitude, km	257	256	256	255	254	253	252
		ΔV, km/s	2.85	2.84	2.84	2.83	2.83	2.83	2.82
		$\overline{I_{sp}}$, s	228	227	227	227	226	226	226
		Residual Propellant Mass, kg	0.00	0.00	0.00	0.00	0.00	0.00	0.03
O/F-	233 kg	Highest Altitude, km	136	139	142	145	138	131	124
		ΔV, km/s	2.61	2.63	2.65	2.67	2.62	2.57	2.52
		$\overline{I_{sp}}$, s	214	214	214	214	213	213	212
		Residual Propellant Mass, kg	2.06	1.32	0.68	0.00	1.29	2.57	3.90

	700 kg	Highest Altitude, km	192	196	199	203	195	187	179
		ΔV, km/s	2.69	2.71	2.73	2.75	2.71	2.66	2.62
		$\overline{I_{sp}}$, s	219	219	219	219	219	218	218
		Residual Propellant Mass, kg	5.02	3.31	1.70	0.00	3.52	7.08	10.85
	2100 kg	Highest Altitude, km	231	235	239	243	235	226	218
		ΔV, km/s	2.73	2.75	2.77	2.79	2.74	2.70	2.66
		$\overline{I_{sp}}$, s	222	222	222	222	222	222	221
		Residual Propellant Mass, kg	15.3	10.1	5.01	0.00	10.4	21.0	31.8
O/F-uncontrolled, Fuel-rich Design	233 kg	Highest Altitude, km	131	134	137	140	142	134	127
		ΔV, km/s	2.58	2.60	2.62	2.64	2.65	2.60	2.55
		$\overline{I_{sp}}$, s	213	213	213	213	213	212	211
		Residual Propellant Mass, kg	2.74	1.98	1.30	0.64	0.14	1.43	2.75
	700 kg	Highest Altitude, km	187	191	194	197	201	193	185
		ΔV, km/s	2.66	2.68	2.70	2.72	2.74	2.70	2.65
		$\overline{I_{sp}}$, s	218	218	218	218	218	218	218
		Residual Propellant Mass, kg	7.04	5.24	3.51	1.87	0.14	3.32	6.97
	2100 kg	Highest Altitude, km	226	230	234	238	241	233	224
		ΔV, km/s	2.70	2.72	2.74	2.76	2.78	2.74	2.69
		$\overline{I_{sp}}$, s	221	222	222	222	222	221	221
		Residual Propellant Mass, kg	20.8	15.8	10.5	5.30	0.15	9.94	20.8

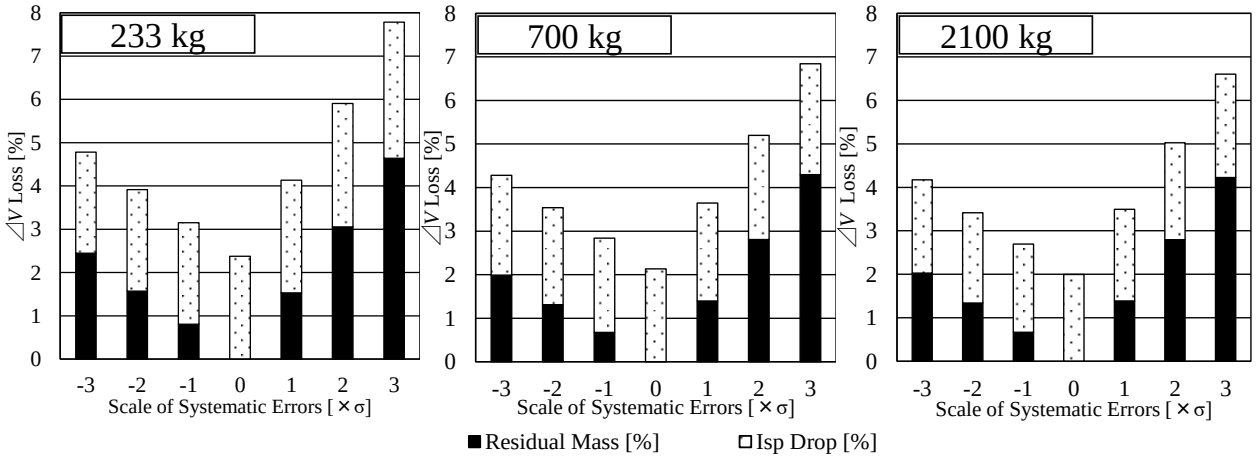

Fig. 11 Breakdown of performance loss in O/F-uncontrolled hybrid rocket simulations.

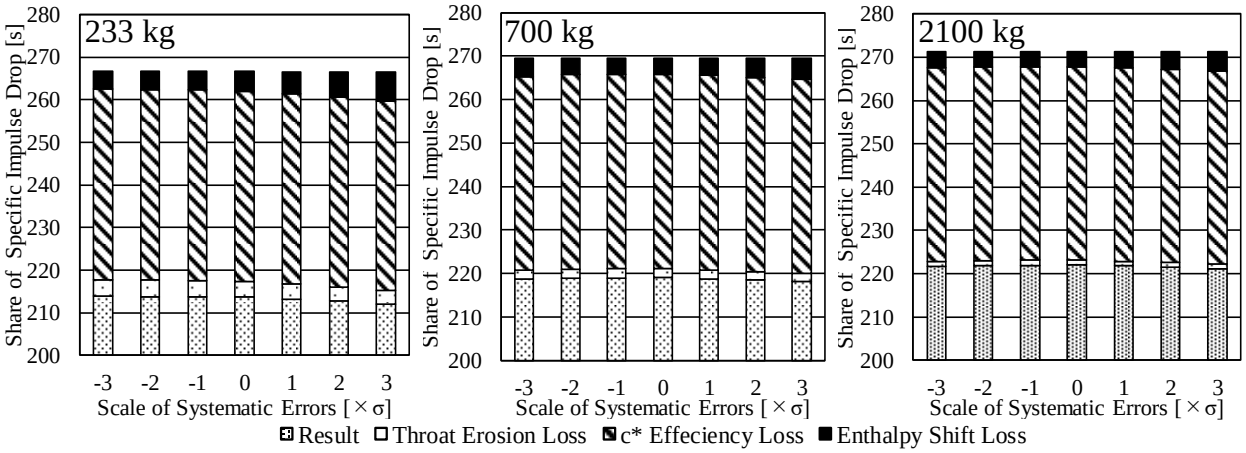

Fig. 12 Breakdown of averaged specific impulse loss in O/F-uncontrolled hybrid rocket simulations.

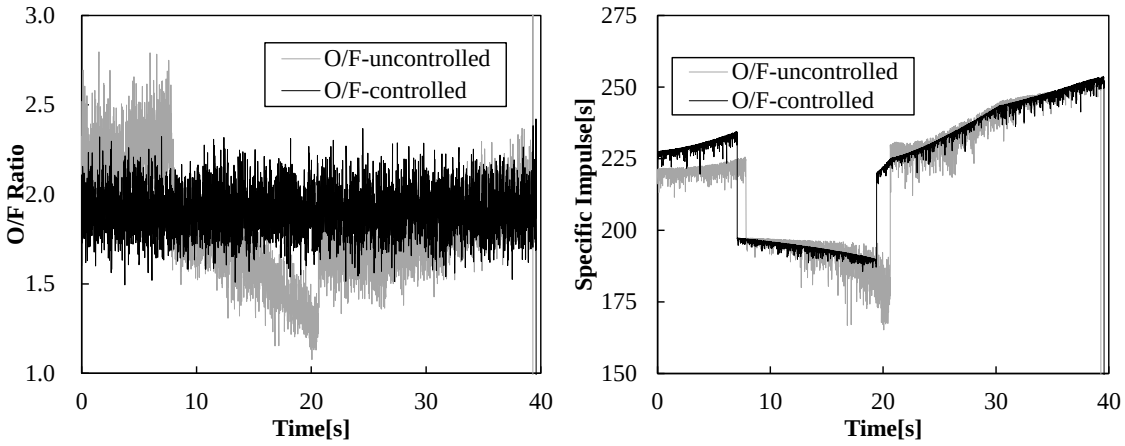

Fig. 13 Typical time-traces of instantaneous O/F and specific impulse.

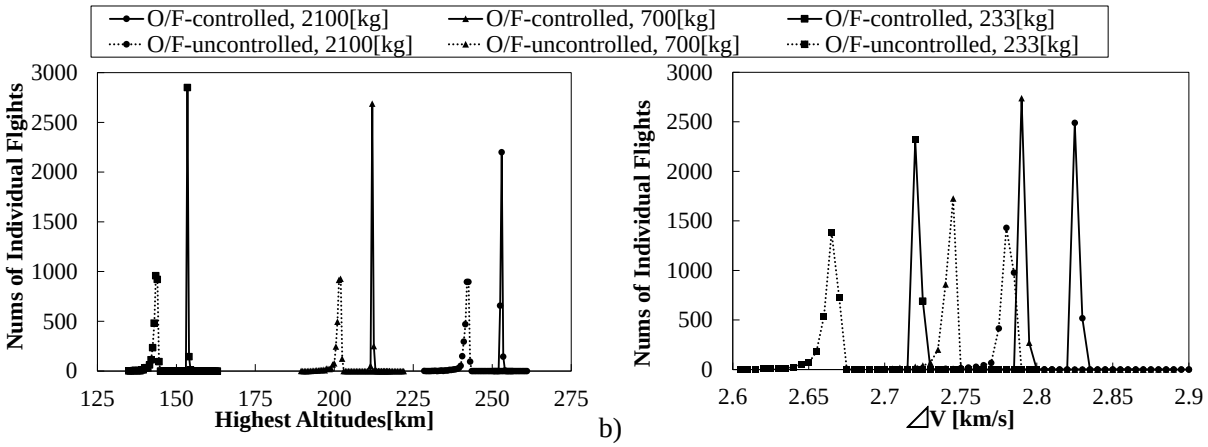

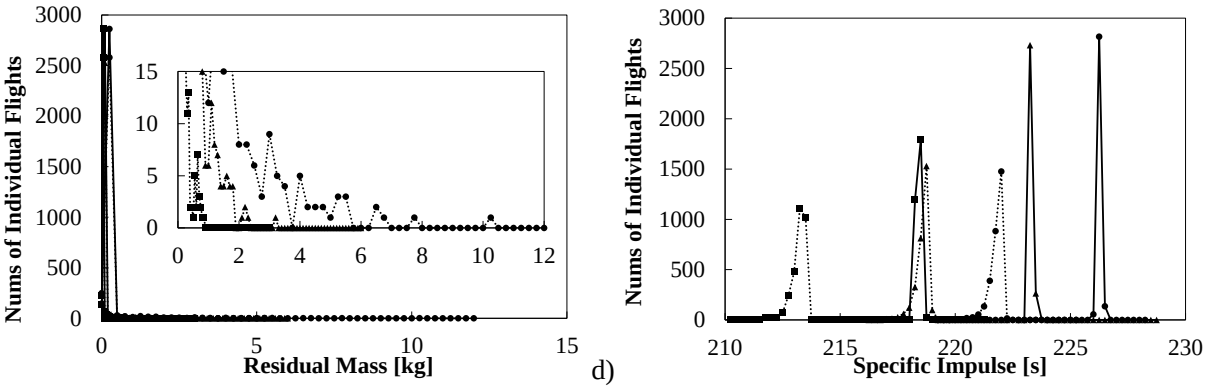

c) d)

Fig. 14 Histograms of flight performance under the fuel regression behavior with random errors: a) highest altitude; b) ΔV; c) residual propellant mass; d) averaged specific impulse.

Table 3 Statistical results of the flight simulations under random errors

		O/F-controlled			O/F-uncontrolled		
		Ave.	Worst	Standard Deviation	Ave.	Worst	Standard Deviation
233 kg	Highest Altitude, km	153	153	0.127	143	135	1.04
	ΔV, km/s	2.72	2.72	7.37×10^{-4}	2.66	2.61	6.83×10^{-3}
	$\overline{I_{sp}}$, s	218	218	5.90×10^{-2}	213	211	0.332
	Residual Propellant Mass, g	1.18	9.71	2.12	15.1	847	67.1
700 kg	Highest Altitude, km	212	211	0.183	201	189	1.21
	ΔV, km/s	2.79	2.79	9.05×10^{-4}	2.74	2.67	6.47×10^{-3}
	$\overline{I_{sp}}$, s	223	223	69.5×10^{-3}	218	216	0.297
	Residual Propellant Mass, g	2.91	30.8	5.75	52.7	3.20×10^{3}	220
2100 kg	Highest Altitude, km	253	252	0.181	241	228	1.24
	ΔV, km/s	2.82	2.82	8.20×10^{-4}	2.78	2.71	5.93×10^{-3}
	$\overline{I_{sp}}$, s	226	226	0.0632	222	220	0.286
	Residual Propellant Mass, g	8.31	94.6	16.5	118	10.1×10^{3}	586